Journal of METAMORPHIC GEOLOGY

# Anti-clockwise pressure-temperature paths record Variscan upper-plate exhumation: example from micaschists of the Porto Vecchio region, Corsica



| | |
|---|---|
| Journal: | *Journal of Metamorphic Geology* |
| Manuscript ID | JMG-17-0010 |
| Manuscript Type: | Original Article |
| Date Submitted by the Author: | 18-Feb-2017 |





| | |
|---|---|
| Complete List of Authors: | Massonne, Hans-Joachim; Universität Stuttgart, Institut für Mineralogie und Kristallchemie<br>Cruciani, Gabriele; Università degli Studi di Cagliari, Dipartimento di Scienze della Terra;<br>Franceschelli, Marcello; Università degli Studi di Cagliari, Dipartimento di Scienze della Terra<br>Musumeci, Giovanni; Universita degli Studi di Pisa, Dipartimento di Scienze della Terra |





| | |
|---|---|
| Keywords: | Corsica, garnet, geochronology, Variscan orogeny, anticlockwise P-T path |

# Anti-clockwise pressure-temperature paths record Variscan upper-plate exhumation: example from micaschists of the Porto Vecchio region, Corsica

**Hans-Joachim Massonne[1], Gabriele Cruciani[2], Marcello Francheschelli[2], Giovanni Musumeci[3]**

[1] Institut für Mineralogie und Kristallchemie, Universität Stuttgart, Germany
[2] Dipartimento di Scienze Chimiche e Geologiche, Università di Cagliari, Italy
[3] Dipartimento di Scienze della Terra, Università di Pisa, Italy

**corresponding author**: H.-J. Massonne, Tel.: +49-711-68581225, Fax: +49-711-68581222, * e-mail: h-j.massonne@mineralogie.uni-stuttgart.de

Short title: **Variscan micaschists of Corsica**

| | |
|---|---|
| Summary: | 282 words |
| Text: | 7483 words (British spelling) |
| References: | 65 |
| Figures: | 11 (colour in print for Figs 1-4, 6, 9-11) |
| Tables: | 4 |

## ABSTRACT

We studied garnet-bearing micaschists which were sampled 3 km east and 15 km northeast of Porto Vecchio, south-eastern Corsica. After a careful investigation of the textural relations and compositions of minerals, especially of zoned garnet, we reconstructed a pressure-temperature (*P-T*) path using contoured *P-T* pseudosections. U-Th-Pb dating of monazite in the micaschists was undertaken with the electron microprobe. The micaschists from both localities formed along similar anti-clockwise *P-T* paths. The prograde branch of these paths starts at 3 kbar close to 600°C in the *P-T* field of sillimanite and reaches peak conditions at 7 kbar and temperatures of 600 (15 km NE of Porto Vecchio) to 630 °C (3 km E of Porto Vecchio). The metamorphism at peak *P-T* conditions happened around 340 Ma based on low Y (< 0.65 wt% $Y_2O_3$) monazite. Ages of monazite with high Y contents (> 2 wt% $Y_2O_3$), which probably have formed before garnet, scatter around 362 Ma. The retrograde branch of the *P-T* paths passes through 4 kbar at about 550°C. We conclude that the studied micaschists belong to a common metasedimentary sequence, which extends over the Porto Vecchio region and is separated from other metamorphic rock sequences in the north and the south by major tectonic boundaries. This sequence had experienced peak pressures which are lower than those determined for metamorphic rocks, such as micaschist and gneiss, from north-eastern Sardinia. At present, we favour a continent-continent collisional scenario with the studied metasedimentary sequence buried during the collisional event as part of the upper plate. The contemporaneous high-pressure metamorphic rocks from NE Sardinia were part of the upper portion of the lower plate. The addressed rocks from both plates were exhumed in an exhumation channel.


KEYWORDS: Corsica, garnet, geochronology, Variscan orogeny, anticlockwise P-T path

## INTRODUCTION

The understanding of metamorphic processes in the Earth's crust requires detailed studies of rock units. These studies should combine geochronological data, the derivation of the pressure (*P*) - temperature (*T*) evolution (= mass flow), and the observation of textural relations (= deformation, melting, etc.) on the mesoscopic and microscopic scale. Recent works, that have followed the above requirements, for instance, in studying metamorphic rock units of the Himalayas, come to the conclusion that the lowermost (nappe) units, which are currently exposed in this orogen, (1) are of Indian affinity, (2) have been exhumed by several relatively discrete, ductile shear-zones, which were active during significantly different times (Middle Eocene to Miocene), and (3) were partially molten enhancing their exhumation (e.g., Liu *et al.*, 2011; Wang *et al.*, 2013; Iaccarino *et al.*, 2015; Carosi *et al.*, 2017 and references therein). The mass flow of the rocks from these (Indian) units can be characterized by clockwise *P-T* loops and back-thrusting near the collisional front although the Indian crust is the lower plate in the corresponding continent-continent collision scenario confirmed by geophysical data (e.g., Zhou & Murphy, 2005).

The aforementioned Himalayas are an orogenic belt with still ongoing continent-continent collision and, thus, active exhumation of the nappe stack at the collisional front. It is easily conceivable that after cessation of the collision this nappe stack will be broadly eroded and other collisional features exposed in a denuded orogen then. This situation exists, for instance, in the Variscan orogen since Permian times according to the evolution of sedimentary cover sequences. Consequently, it is reasonable to study collisional processes, deeply located in orogenic crust, in the (Carboniferous) Variscan basement instead of that in the Himalayas. Integrated studies considering geochronology, metamorphic petrology, and structural geology, as suggested above, were already undertaken by various authors in the Variscan basement (e.g., Giacomini *et al.*, 2008; Cruciani *et al.*, 2016, in the here addressed

Corsica-Sardinia block). However, geodynamic conclusions, resulting from the work in this basement, suffer from the unclear location of the former collisional front and geometry of the colliding plates which is easy to reconstruct for an ongoing continent-continent collision as in the Himalayas.

In the north-eastern part of the Variscan Corsica-Sardinia block, high-pressure (HP: >10 kbar) metamorphic rocks occur (see below) that reflect collisional processes affecting the upper portion of the downgoing continental plate. In this paper, we report about metamorphic rocks which are part of the upper plate, but are now in tectonic contact to the HP ones from the lower plate. The studied rocks are characterized by an anti-clockwise *P-T* path which could be typical for the lower portion of the upper plate exposed in denuded orogens.

## GEOLOGICAL SETTING

### General aspects

The Corsica-Sardinia block represents a major area of exposed Variscan crust in south-western to central Europe (Faure *et al.*, 2014; Rossi *et al.*, 2009). This area is traditionally subdivided into the Inner Zone (or Axial Zone), exposed in northern Sardinia and Corsica, and the Internal and External Nappe zones of central to southern Sardinia (Ghezzo & Orsini, 1982; Carmignani *et al.*, 1994; 2001 and references therein). Late Carboniferous batholiths (Rossi & Cocherie, 1991; Paquette *et al.*, 2003) of various granitoids dominate the Inner Zone but minor coherently exposed areas of medium- to high-grade metamorphic rocks occur as well (e.g. Ménot & Orsini, 1990; Fig. 1). Sardinian metamorphic rocks north of the Posada-Asinara line (PAL), a major strike-slip fault in northern Sardinia, are characterized by HP metamorphism: (1) eclogite bodies, enveloped by gneisses, occur in north-eastern Sardinia (Cortesogno *et al.*, 2004; Cruciani *et al.*, 2011, 2012, 2015; Franceschelli *et al.*, 2007; Giacomini *et al.*, 2005); (2) the country rocks, various types of gneisses and migmatites frequently with some garnet, experienced pressures slightly in excess of 10 kbar (Cruciani *et al.*, 2008a, b; Massonne *et al.*, 2013); (3) the peak pressure recorded by micaschists can even be as high as 17 kbar (Cruciani *et al.*, 2013). The occurrences of HP metamorphic rocks extend to south-eastern Corsica where granulites are exposed which had experienced pressures as high as 19 kbar (Giacomini *et al.*, 2008).

U-Pb zircon ages obtained from the cited HP rocks were related to HP (or high-temperature) metamorphism as follows: Early Devonian ages were reported by Cortesogno *et al.* (2004: 403 ± 4 Ma) and by Palmeri *et al.* (2004: 400 ± 10 Ma). Late Devonian to Early Carboniferous ages were given by Giacomini *et al.* (2005: 352 ± 3 Ma; 2008: 361 ± 3 Ma). These authors suggested a long-lasting exhumation of the HP rocks from south-eastern Corsica in Early Carboniferous times (c. 360-330 Ma) accompanied by a deformational event (D2 according to Giacomini *et al.*, 2008). Later on (315-325 Ma, D3) shear zones such as the PAL became active (Di Vincenzo *et al.*, 2004; Carosi *et al.*, 2012). These shear zones are widespread in the Corsica-Sardinia block (Elter *et al.*, 1990, 1999) and characterized by an orogen-parallel, dextral transpressive regime (Carosi & Oggiano, 2002; Carosi & Palmeri, 2002; Iacopini *et al.*, 2008).

**Sampling areas**

In the sampling area east of Porto Vecchio (Fig. 1a,b), the Palaeozoic basement mainly consists of Late Carboniferous granodiorite and syenogranite of the Corsica-Sardinia batholith (Rossi & Cocherie, 1991). A large slice of amphibolite-facies metamorphic rocks (Porto Vecchio Unit) is embedded in these magmatic rocks (Rouire *et al.*, 1993). The Porto Vecchio Unit is a sequence of metasediments and orthogneisses characterized by upright (steeply dipping) NW-striking lithological boundaries and metamorphic foliations. We sampled these rocks along the Route de Phare (Fig. 1b). In this work, we focus on the two-mica paragneiss which includes decimetre to metre thick layers of garnet-bearing micaschist. The fine- to medium-grained paragneiss consists of quartzofeldspathic layers alternating with thin biotite-muscovite-rich layers marked by the diffuse presence of muscovite porphyroblasts. The micaschist, such as our sample Cors15G, is characterized by biotite-rich layers with diffuse occurrence of millimetre-sized garnet porphyroblasts that also occur in micaceous layers within the paragneiss. This metasedimentary sequence is characterized by two sets of foliation with a dominant well-developed mylonitic fabric at the outcrop scale. This fabric is due to the activity of a major shear zone, the Porto Vecchio Shear Zone (PVSZ, Fig. 1b).

Adjacent to the micaschist-paragneiss sequence to the north a mylonitic orthogneiss occurs which is well exposed along the coast of the Punta Chiappa area. This rock is characterized by centimetre to decimetre thick quartzofeldspatic-rich layers, showing a transition from decimetre to metre thick domains with augen fabric, and alternating biotite-rich layers. According to our observation, a N 110° - 130° E steeply dipping mylonitic foliation is present. A dextral sense of shear (Fig. 1b) can be derived from asymmetric porphyroclasts and SC-type shear bands of decimetre to centimetre size. A previous older gneissic foliation is recognizable in the less deformed domains. This rock fabric, which relates to the activity of the PVSZ, is compatible with that reported by Giacomini *et al.* (2008).

The southern part of the Fautea-Solenzara Unit crops out in our sampling area ~15 km north-east of Porto Vecchio (Fig. 2). This unit is made up of granulite, migmatite, gneiss, and micaschist (Rouire *et al.*, 1993). The latter two rock types dominate at and near Punta di Fautea and suggest a metasedimentary sequence also because of the interlayering of white-mica and quartz-rich rocks. The finely foliated rocks there show a clear folding of the foliation planes (Fig. 2b). Especially in gneiss stretched and asymmetric quartz-feldspar porphyroclasts occur pointing to shearing as well. In micaschist a diffuse occurrence of mm-sized garnet, frequently in layers of mm-sized biotite and potassic white-mica, is obvious (samples Cors16 and Cors17). Occasionally, cm-sized garnet appears (Fig. 2c).

## ANALYTICAL PROCEDURES

In order to analyze the three micaschist samples Cors15G, Cors16, and Cors17 for major elements, finely ground rock powder was produced from a small rock block, c. 20-30 g, which was previously used for the preparation of polished thin-sections. A glass disk was prepared by fusing rock powder with Spectromelt® (ratio 1:6). This disk was analyzed with a PHILIPS PW2400 X-ray fluorescence (XRF) spectrometer with wave-length dispersive (WD) system. Three standards were measured before the samples to verify that the calibration of the instrument was still alright.

For the chemical analysis of minerals in our samples a CAMECA SX100 electron microprobe (EMP) with 5 WD systems was employed. The conditions for a c. 2 minutes lasting analysis of a silicate or ilmenite, including the analytical errors, were reported by Massonne (2012). For the calculation of structural formulae of minerals and the content of molar fractions of mineral components from EMP analyses, the computer programme CALCMIN (Brandelik, 2009) was used.

For dating of monazite with the EMP, Si, P, S, Ca, Y, La, Ce, Pr, Nd, Sm, Eu, Gd, Pb (for peak and background altogether c. 20 min. counting time), Th, and U were analyzed following the approach of Massonne *et al.* (2012). This procedure yields a good match with more precise mass spectrometric methods for dating of Tertiary to Palaeozoic monazite (see Massonne, 2016a; Waizenhöfer & Massonne, 2017). The 2σ uncertainty of our dating results related to a single analysis was calculated by error propagation of the 2σ errors of the counting rates of the peak and background intensities of the relevant elements. Since many monazite analyses yielded $ThO_2$ contents between 4 and 5 wt% and $UO_2$ contents close to 1 wt%, a 1σ error between 6 and 7 Ma often resulted for the single analysis. The determination of the monazite ages were undertaken with the CALCMIN programme (Brandelik, 2009).

Errors were calculated with the MINCALC-V5 software programme (Bernhardt, 2007). The Isoplot programme of Ludwig (1999) was used to calculate average ages and errors of monazite populations.

To recognize zoning patterns of garnet, potassic white mica, and monazite, five element concentration maps for major and minor elements were prepared simultaneously by step-wise movement of a thin section under the electron beam of the EMP and subsequent computer-aided evaluation. For the mapping, counting times per step of 100 ms were applied. The electric current was either 50 nA (monazite, garnet) or 25 nA (mica).

## MINERAL TEXTURES AND COMPOSITIONS

The studied micaschists (Cors15G, Cors16, Cors17) were taken from rock portions without evidence of partial melting. The major and minor minerals in these rocks are quartz, white mica, biotite, plagioclase, garnet, and sillimanite. Accessory phases are apatite, monazite, zircon, opaque phases (mainly ilmenite), and K-feldspar (found only in Cors17).

Micas form two main generations which both are hardly oriented but enriched in layers with thicknesses less than 1 cm. The older generation is characterized by mm-sized, thick flakes (Fig. 3a) which can be bent and kinked (Fig. 3c). The younger main generation, typically showing undeformed grains with sizes around 0.1 mm, frequently surrounds these flakes (Fig. 3a). Aggregates of very fine-grained (frequently <10 μm) micas (third generation), which are mostly potassic white-mica, occur (Fig. 3f). Occasionally, elongated clusters of sillimanite (fibrolite) are in the centre of these mica aggregates (Fig. 3e). These clusters can be bent (Fig. 3e).

Layers enriched in quartz and plagioclase occur. Larger plagioclase grains (Fig. 3d) can be partially surrounded by significantly smaller grains of this phase. Originally existing larger quartz grains, experienced, however, a complete grain size reduction.

Most garnet grains show diameters less than 0.5 mm (Fig. 3d). These grains are well preserved in contrast to mm-sized garnet in sample Cors15G, which are broadly decomposed. The decomposition products resemble pinite (Fig. 3b). However, garnet relics in the "pinite" aggregate clearly prove that it formed from this mineral instead of cordierite. True inclusions in garnet are quartz and ilmenite. In case of some micas, they can also be decomposition products instead of inclusion phases.

Mineral abundances were determined counting "pinite" and aggregates of very fine-grained micas as garnet and sillimanite, respectively. Garnet modal contents in the three samples are about 2 vol%. Sillimanite contents are different (c. 1-2 % in Cors15G and Cors17, 10 % in Cors16). Mica contents are 40-45, 45-48, and 35 % in samples Cors15G, Cors16, and Cors17, respectively. Potassic white mica predominates. Ratios of white to dark mica are between 4:1 (Cors16) and 2:1 (Cors17). Quartz contents are between 40 (Cors16) and 50 %. Plagioclase modal contents amount to 10-15 % in samples Cors15G and Cors17. Sample Cors16 contains only a few percent plagioclase. Ilmenite contents are around 0.5 %.

A compositional variability of garnet in samples Cors15G and Cors17 is discernable in the elemental maps of Figure 4. Results of EMP spot analyses of the diverse garnet domains are shown in Figure 5 and Table 1. The composition of the garnet core (with idiomorphic shape in Fig. 4) in sample Cors17 is, in terms of molar fractions, $Alm_{0.735}Gro_{0.04}Pyr_{0.125}Spe_{0.10}$ (with components Alm: almandine, Gro: grossular (+andradite), Pyr: pyrope, Spe: spessartine). The mantle tends to higher spessartine and lower pyrope and grossular contents. The composition of the garnet rim is $Alm_{0.725}Gro_{0.025}Pyr_{0.10}Spe_{0.15}$. The mm-sized garnet in sample Cors15G, although corroded, has extended cores with a prograde zonation (inner core region: $Alm_{0.70}Gro_{0.04}Pyr_{0.145}Spe_{0.115}$, outer core region: $Alm_{0.73}Gro_{0.04}Pyr_{0.16}Spe_{0.07}$), i.e. decreasing Mn and slightly increasing Mg contents. A poorly defined mantle ($Alm_{0.75}Gro_{0.04}Pyr_{0.15}Spe_{0.06}$) surrounds this core. After significant corrosion of such large garnets, a Mn-rich garnet rim ($Alm_{0.715}Gro_{0.045}Pyr_{0.06}Spe_{0.18}$) grew around the remaining fragments (Figs. 4 and 5, Table 1).

Potassic white-mica in the three studied samples is exclusively muscovite. However, the texturally different muscovite generations can be compositionally distinguished (Figs. 6 and 7, Table 2). The oldest generation (thick flakes) contains considerable amounts of Ti (around 1 wt% $TiO_2$). Contents of Si per double formula unit (pdfu) slightly scatter around 6.08 in Cors15G and 6.12 in Cors17. In the elemental maps of Figure 6 domains with somewhat higher Ti (and Mg according to the substitution 2 Al = Mg + Ti) or Na are discernable. The younger mica generation (smaller flakes around the thick flakes), as worked out for Cors17 (Fig. 7), is characterized by lower Ti contents (<0.4 wt% $TiO_2$) and somewhat higher Si contents (around 6.17 Si pdfu) compared to the oldest white mica generation. In Cors15G, slightly larger grains in the aggregates of very fine-grained micas could be analyzed. These grains are characterized by very low Ti contents and Si around 6.30 pdfu. The contents of Mg and Fe are relatively high due to the Tschermak's substitution (Si + Mg,$Fe^{2+}$ = 2 Al).

The characteristics of large biotite flakes (oldest generation) are: Si per formula unit (pfu) = 2.63 in Cors15G and 2.65 in Cors17, $X_{Mg}$ = Mg/(Mg+Fe+Mn) = 0.38 in Cors15G and 0.41 in Cors17, and Ti as $TiO_2$ in wt% = 2.7 in Cors15G and 2.4 in Cors17. The small flakes of the second mica generation in Cors17 show a lower $TiO_2$ content of about 1.1 wt%. $X_{Mg}$ (0.42) is only slightly above that of the large flakes.

Plagioclase in the studied micaschists is oligoclase with anorthite contents of 21-22 mol% in Cors15G and 16 mol% in Cors17. K-feldspar contents are 2.5 mol% in Cors15G and around 1.5 mol% in Cors17. The composition of K-feldspar found in Cors17 is close to that of the ideal end-member (Table 2).

## PRESSURE-TEMPERATURE EVOLUTION

**Applied method**

We calculated *P-T* pseudosections with the PERPLE_X computer programme package (see Connolly, 2005; version from August 2011 downloaded from the internet site http://www.perplex.ethz.ch/) to derive the *P-T* evolution of the micaschists. The *P-T* range of 1-16 kbar and 400-700 °C, the system Si-Ti-Al-Mg-Mn-Fe-Ca-Na-K-H-O, and the thermodynamic data set of Holland & Powell (1998, updated 2002) for $H_2O$ and minerals, which were pure phases, such as rutile and clinozoisite, and various solid-solutions described by the following models (see the PERPLE_X file solution_model dat), were considered: (1) TiBio(HP) for biotite being identical to the previous model Bio(HP) of Powell & Holland (1999) as the tbi component was excluded (see below), (2) Chl(HP) for chlorite based on the formulation by Holland *et al.* (1998), (3) Ctd(HP) for chloritoid ("from THERMOCALC", written comm. by J.A.D. Connolly), (4) feldspar for ternary feldspar according to Fuhrman & Lindsley (1988), (5) Gt(HP) for garnet (Holland & Powell, 1998) with maximal 60 mol% spessartine component, (6) Opx(HP) for orthopyroxene (Powell & Holland, 1999), (7) Mica(M) for paragonite (Massonne, 2010) with maximal 50 mol% muscovite component, (8) Pheng(HP) for potassic white mica (see Powell & Holland, 1999, as well as comments in file newest_format_solut.dat) with maximal 50 mol% paragonite component, and (9) St(HP) for staurolite ("from THERMOCALC", written comm. by J.A.D. Connolly). In fact, we used older solid-solution models for clinopyroxene and amphibole, Omph(HP) based on the thermodynamic data given by Holland & Powell (1996), augmented by those of the end members aegirine and $CaAl_2SiO_6$ (see Zeh *et al.*, 2005), and GlTrTsPg (glaucophane-tremolite-tschermakite-pargasite + corresponding $Fe^{2+}$-bearing components, Powell & Holland, 1999), but these phases turned out to be not of relevance for the here derived P-T conditions. For cordierite and ilmenite the ideal solid-solution models hCrd and IlGkPy (max. 30 mol% geikilite component), respectively, were used, which are based on the thermodynamic data for corresponding end-members given by Holland & Powell (1998). The amphibole end-members acti, cumm, and grun, the abbreviated end-member phases ann1, mic (microcline), and ab (low T albite), and the $O_2$ buffers qfm and mthm in the applied data file were not considered. Both Ti end-members tip and tbi in white and dark micas, respectively, were excluded because of their untrustworthiness (see, e.g., discussion in Massonne, 2012).

The bulk-rock compositions of the micaschists (Table 3), determined by XRF, were modified for the PERPLE_X calculations: (1) The CaO content was reduced because some Ca is bound to apatite, $Ca_5(PO_4)_3(OH,F)$. Since several larger grains (see below) of monazite, $(Ce,La)PO_4$, were found besides apatite grains in each thin section of the micaschists, we considered that a CaO content equivalent to two third of the analysed content of $P_2O_5$ in the bulk-rock was bound to apatite and correspondingly subtracted from the bulk-rock for the PERPLE_X calculations. In order to check the influence of this modification on the *P-T* results for our Ca-poor bulk-rock compositions, we also achieved a calculation for CORS17 without this modification. (2) The oxygen content, which is related to the amount of trivalent iron in the rock, can have a significant influence on the *P-T* results of medium to high temperature metapelites (Massonne, 2014). However, in the micaschists $Fe^{3+}$ only occurs in very minor amounts in silicates (see garnet compositions in Table 1). Therefore, we estimated that less than 5 % of the iron was trivalent during metamorphism. Consequently, the PERPLE_X calculations were undertaken either without $O_2$ or a small $O_2$ content equivalent to 5 % of the iron being trivalent to check the influence of such small amounts of $Fe^{3+}$ on our *P-T* calculations. (3) A water content of 5 wt% was considered to permit the formation of a free hydrous fluid already at the lowest temperatures of our calculations. In one case, only 1.95 wt% $H_2O$ was added to the dry bulk-rock composition to check the effect of water-undersaturated conditions at retrograde metamorphic conditions (for more details, see below). (4) For all PERPLE_X calculations, the sums of the oxide contents were normalized to 100 wt% (Table 3). For a late metamorphic stage, effective bulk-rock compositions are often considered, for instance, by subtracting garnet cores from the bulk-rock (e.g., Groppo &

Rolfo, 2008) although this has little effect even at significantly higher garnet contents than 2 vol.% as in our rocks (e.g., Massonne, 2014, 2016a; Waizenhöfer & Massonne, 2017). As the garnet grains are usually partially decomposed (Fig. 4), the garnet cores were clearly involved in retrograde reactions (already at high temperatures - see below) so that we considered the entire bulk-rock composition as being (nearly) effective during the entire metamorphism.

The obtained *P-T* pseudosections were contoured by isopleths for molar fractions of garnet components, Si contents in potassic white mica and modal contents of garnet. Such isopleths were used to obtain metamorphic *P-T* data.

## Calculation results and *P-T* path

The obtained *P-T* pseudosections (Fig. 8) for the five modified bulk-rock compositions with 5 wt% $H_2O$ (Table 3) resemble each other and those calculated (e.g., Massonne & Toulkeridis, 2012; Massonne, 2016a; Waizenhöfer & Massonne, 2017) for metamorphosed relatively immature clastic sediments (bulk-rock compositions according to XRF analyses: $SiO_2$ = 58-72 wt%, CaO < 1 wt%, $K_2O$ > 3 wt%, $Na_2O$ > 0.8 wt%, $Al_2O_3$ = 15 -21 wt%, considerable Fe and Mg contents) at medium metamorphic grade (450-650 °C, 2-16 kbar). Typical features in such pseudosections for the given *P-T* range are (1) the omnipresence of potassic white-mica (except at the lowest pressures and highest temperatures) and quartz, (2) the limitation of cordierite to pressures below 3.5 kbar, resulting only occasionally in an overlap of the P-T fields of cordierite and garnet (see Massonne, 2016a), (3) the appearance of a $Al_2SiO_5$ polymorph (andalusite or sillimanite) above 500-550 °C at 2-3.5 kbar and its (sillimanite, kyanite) disappearance between 7 (see Fig. 8) and 9 kbar (see Massonne, 2016a, also shown for Ca-richer metapelites by Jeřábek *et al.*, 2008) at 650 °C (for Cors17: c. 8.5 kbar), (4) the occurrence of a small P-T field for staurolite (typically as shown in Fig. 9), and (5) a maximum pressure for ilmenite between 8.5 and 14 kbar (Cors17, see also Waizenhöfer & Massonne, 2017) at a temperature ≥ 550 °C. In addition, the occurrence of biotite and plagioclase can be limited to pressures of 10 kbar at temperatures around 600 °C. However in case of micaschists Cors15G and Cors17, these upper pressure limits are clearly above 10 kbar. At temperatures above 450°C, the mineral phases lawsonite, chloritoid and (Na rich) amphibole typically appear at HP conditions only (see Fig. 8a).

The variation of the composition of garnet and potassic white-mica in the aforementioned medium-grade metamorphic rocks is likewise. The pyrope content in garnet increases with rising temperature or, at pressures below approximately 10 kbar, rising pressure at temperatures above 600°C (Fig. 8b). At these temperatures, the grossular content increases with pressure (up to 13-14 kbar). However, at HP conditions this increase results rather from falling temperatures (Fig. 8b). The Si contents in potassic white-mica increase with rising pressure (Fig. 8c), but this increase is moderate for low Si contents (6.0-6.1 pdfu) compared to higher Si contents above c. 550 °C. For this reason, barometry with Si in potassic white-mica is fairly insensitive at corresponding *P*-*T* conditions for the above considered metasediments. Thus, the derivation of these conditions in the following is based mainly on the compositional and modal characteristics of garnet.

The consideration of some $Fe^{3+}$ (5% of the total iron) in the bulk rock composition (Table 3) has a minor effect (shift by a few degrees only) on the *P*-*T* position of the kind of isopleths, which are exemplarily shown in Figure 8, for the *P*-*T* range (see below: $T > 500$°C, $P < 10$ kbar) relevant for our micaschists (Cors15G and Cors17). The difference between the *P*-*T* limits of specific mineral phases in calculations without and with some $Fe^{3+}$ can also be very small (see the staurolite fields in Fig. 9b). This concerns the limit for garnet below 7 kbar as well. However, at higher pressures ($T < 520$°C) a larger *P*-*T* difference of the garnet limit is discernable in Figure 9b. A considerable shift of the garnet isopleths for XCa toward lower pressures (or higher *T*) is notable when the Ca correction for apatite is not applied (Fig. 9b). This correction might be particularly critical for the thermodynamic modeling using garnet in apatite-bearing rocks with low CaO content in the bulk rock. For this reason, Cors16 (Table

3) was not modelled. Other kinds of isopleths considered here (XMg, XMn, vol% of garnet, Si in muscovite) are hardly affected. The *P-T* field of garnet is somewhat extended at higher CaO contents in the bulk-rock (Fig. 9b).

The compositional trend of garnet in Cors17 (Figs. 4 and 5) results in the *P-T* conditions, marked by the grey ellipses in Figure 9b, when some $Fe^{3+}$ in the bulk rock is considered and the Ca correction for apatite is ignored. The peak *P-T* conditions derived from the garnet core composition $Alm_{0.735}Gro_{0.04}Pyr_{0.125}Spe_{0.10}$ are close to 7 kbar and 600°C. The inner garnet mantle composition $Alm_{0.71}Gro_{0.045}Pyr_{0.115}Spe_{0.13}$ points to a slight temperature decrease at constant pressure. At this stage, the calculated garnet volume is 2 vol.% as observed (see above). The calculated contents of anorthite in plagioclase and Si in biotite are 15.5 mol% and 2.685 pfu, respectively, which are close to the analysed values (Table 2). The compositions of large muscovite flakes (oldest generation) reach Si contents close to 6.20 pdfu (Fig. 7), compatible with the peak pressure conditions, but the majority is lower in Si (down to 6.05 pdfu) and, thus, should have formed at lower pressures and relatively high temperatures (e.g., 3.5 kbar and 580°C). The same should apply for sillimanite (relics) because the derived peak *P-T* conditions are already outside the *P-T* field of sillimanite (Fig. 9b). The subsequent compositional evolution towards the garnet rim ($Alm_{0.725}Gro_{0.025}Pyr_{0.10}Spe_{0.15}$) points to decreasing pressure and temperature to 4.5 kbar and 565-570 °C. The derivation of the *P-T* conditions using the calculation result for the bulk-rock composition of Cors17 without $Fe^{3+}$ and Ca correction (red ellipses in Fig. 9b) yields slightly higher peak pressures (less than 0.2 kbar) compared to the result with $Fe^{3+}$ in the bulk-rock.

Similar *P-T* conditions were determined from the study of micaschist Cors15G. However, the P-T trajectory is a prograde one using the compositional trend of the extended garnet core (although strongly corroded) in this rock (Fig. 5). The XCa and XMg isopleths for the outer core composition ($Alm_{0.73}Gro_{0.04}Pyr_{0.16}Spe_{0.07}$) and that for a garnet modal content of 2 vol% intersect at about 7 kbar and 630°C (Fig. 9a) using the bulk-rock composition with no $Fe^{3+}$ and Ca correction for apatite. Applying additionally to XCa and XMg isopleths those for XMn, the deducible prograde path starts, based on the inner core composition ($Alm_{0.70}Gro_{0.04}Pyr_{0.145}Spe_{0.115}$), at approximately 5.5 kbar and 615°C, when we take into account that the XCa = 0.04 isopleth, as shown in Figure 9a, would shift to lower pressures if this Ca correction is neglected. These P-T conditions as well as those at still lower pressures (e.g. 3.5 kbar and 580°C) agree with the formation of sillimanite in Cors15G (Fig. 3e) and the dominance of muscovite with Si contents around 6.08 pdfu (Fig. 7). Again the contents of anorthite in plagioclase and Si in biotite (18 mol% and 2.625 pfu), calculated for the peak *P-T* conditions, are compatible with analysed values (Table 2). However, the calculated Si content in biotite at 3.5 kbar and 580°C is only 2.51 pfu. Although, the garnet mantle compositions with Mg contents lower than that of the outer core (Fig. 5) point already to slightly reduced temperatures, the garnet rim composition ($Alm_{0.715}Gro_{0.045}Pyr_{0.06}Spe_{0.18}$) was thought to be helpful in determining the *P-T* conditions of a late metamorphic stage. Unfortunately, the corresponding XCa and XMg isopleths intersect somewhat outside the *P-T* field of garnet (Fig. 9a) at approximately 530 °C and 3.5 kbar. We followed the idea that a deficit of $H_2O$, typical for retrograde conditions, could bring this intersection into a more extended garnet field. Therefore, we calculated several pseudosections for Cors15G with various $H_2O$ deficits. Even a slight deficit as given in Table 3 (see also the V out curve in Fig. 9a) leads, in fact, to a significant extension of the garnet field to lower temperatures, but the relevant XMg = 0.06 isopleth is also shifted to rather unlikely low temperatures for retrograde garnet formation (Fig. 9a). Another approach to define *P-T* conditions of the retrograde *P-T* trajectory was applied considering the very small white-mica grains with Si = 6.30 pdfu. However, a corresponding retrograde temperature can only be roughly estimated. As biotite has formed together with this white mica the minimum temperature could be as low as 400 °C (see breakdown curve of biotite in Massonne & Willner, 2008) or still less depending on pressure (Massonne, 2010; this work). As virtually no chlorite occurs in Cors15G higher temperatures than 400°C seem to us to be likely. Nevertheless, we estimated c. 400°C and 3 kbar as possible retrograde conditions.

The thermodynamic modeling for micaschists Cors15G and Cors17 results in anti-clockwise *P-T* paths (Fig. 9), which have a hair-pin shape close to the peak *P-T* conditions of 7 kbar and 630 (Cors15G) or 600 °C (Cors17).

## DATING RESULTS OF MONAZITE

Monazite appears as rather large grains in both micaschists, Cors15G and Cors17. Several grains with sizes above 50 µm were found in each studied thin-section. The maximum size was about 200 µm (see Fig. 10). In back-scattered electron (BSE) images, obtained with the EMP, complex zonations are discernable. From a few monazite grains, elemental maps (Ca, Y, Ce, Gd, Th) were produced. The most obvious zonations can be recognized in Y maps (Fig. 10). Spot analyses (Cors15G: 21 grains, 38 analyses; Cors17: 17 grains, 35 analyses) lead to a chemical characterization of various monazite domains and U-Th-Pb ages (Table 4). The results are presented in Figure 10 in terms of $Y_2O_3$ content in wt% and the La/Gd and Th/U ratios plotted versus the age.

The obtained 73 ages scatter between 328 and 384 Ma (Fig. 10). Especially the Y contents in monazite vary significantly and, thus, allow a chemical discrimination of monazite domains, which are already discernable in Y maps of monazite. In Figure 10c, three such domains of low, medium, and high Y contents can be recognized. Accordingly, we arbitrarily defined two Y limits (see Fig. 10e) to discriminate between monazite populations. Using the Isoplot programme, the ages of these populations are: 362.2 ± 4.1 (2σ, 95% confidence level) Ma (mean square of weighted deviates = MSWD: 2.7) for the high-Y population, 350.8 ± 4.2 Ma (MSWD: 1.7) for the medium-Y population, and 340.5 ± 4.4 Ma (MSWD: 2.7) for the low-Y population. As the three oldest ages of the latter population are characterized by unusual high Th/U ratios, we recalculated the age for this population without these three data; an age of 337.1 ± 2.8 Ma (MSWD: 1.0) resulted. The three populations are characterized by mean La/Gd ratios of 9.9 (high Y), 12.2 (medium Y), and 20.2 (low Y). The Th/U ratios of the analyzed monazite scatter around 6 (Fig. 10e).

## DISCUSSION

### Metamorphic evolution

According to the above outlined derivation of metamorphic conditions for the studied micaschists Cors15G and Cors17, representing a metasedimentary sequence of two basement areas near Porto Vecchio (Figs. 1 and 2), the peak *P-T* conditions could be well constrained. Peak pressures are close to 7 kbar. Peak temperatures were 630 °C regarding the area at Punta di a Chiappa, a few km east of Porto Vecchio, whereas 600 °C resulted for the area at Punta di Fautea, 15 km north-east of Porta Vecchio. In fact, prograde and retrograde paths to and from peak conditions could be less well constrained, but these branches of the *P-T* paths seem to be at least similar for both study areas (Fig. 9). On the basis of these paths and our textural observations (section MINERAL TEXTURES AND COMPOSITIONS), a consistent picture for the evolution of the studied metamorphic rocks can be reconstructed: At about 3 kbar (c. 12 km Earth depth) and 550-600 °C, relatively coarse-grained (grain sizes around 1 mm) micaschists, consisting mainly of quartz, plagioclase, muscovite (Si pdfu: 6.06-6.10), biotite, and sillimanite, had formed in a regional environment characterized by high geothermal gradients of 45-50 °C/km. During the subsequent burial to depths of c.25 km (*P* of 7 kbar) garnet started to grow and occasionally formed porphyroblasts (Figs. 2c, 3b). Probably before reaching peak *P-T* conditions a major deformation event occurred leading, for instance, to growth of relatively small micas at the expense of stressed palaeograins of both biotite and muscovite. Contents of Si in the newly formed muscovite are correspondingly higher (e.g., 6.16 pdfu in Cors17, see Fig. 7) than in the palaeograins. Replacement of sillimanite by fine-grained muscovite started probably at this stage, but continued during exhumation (retrograde path) under formation of very-fine grained micas (Fig. 3e). At the very early retrogression (soon after passing the *P-T* peak) garnet was corroded and replaced by retrograde garnet (Cors17), i.e. garnet richer in Mn than the early prograde garnet, or by micas (Cors15G). The latter replacement feature was probably caused by fluid infiltration resulting in a significant corrosion of garnet to form pinite-like mica aggregates (Fig. 3b). Even in such aggregates a slight re-growth of relatively Mn-rich garnet (Fig. 5a) happened. This event was assigned to *P-T* conditions of 530 °C and 3.5 kbar (see above).

The anti-clockwise path with hair-pin shape, which is consistent with the textural and chemical evolution of the micaschist minerals, is in clear contrast (see Fig. 9c) to the clockwise *P-T* path of Giacomini *et al.* (2008) suggesting clearly higher pressures (at least 9 kbar) at the beginning of the recorded metamorphic evolution, higher peak temperatures (>650 °C), and lower pressures (1-2 kbar) at a late metamorphic stage ($T$ > 500 °C) compared to our path. To appraise this clockwise path, it must be noted that Giacomini *et al.* (2008) considered broadly the change of mineral assemblages and, to a limited extend, mineral compositions, such as the Si content in potassic white mica (< 6.2 pdfu as hint at $P$ < 5 kbar - compare with Fig. 9a), for their *P-T* estimations. Only one calculation with THERMOCALC was presented by these authors for the assemblage biotite-muscovite-garnet-sillimanite-plagioclase resulting in *P-T* conditions of 5.2 kbar at 660°C, which might be within errors even compatible with our *P-T* estimates. However, it is not clear which mineral compositions were used by Giacomini *et al.* (2008) to obtain this *P-T* datum. Therefore, we suspect that the mineral compositions applied by these authors were not in equilibrium. According to our *P-T* paths, garnet and sillimanite were in equilibrium only in a narrow *P-T* range (for Cors15G around 5 kbar and 610 °C, see Fig. 9a). According to Giacomini *et al.* (2008), the early retrograde path proceeded at very low pressures (Fig. 9c). However, this view, which is in contrast to our findings, might have resulted from the error that the "pinite" aggregates (see above) represent retrogressed cordierite. In addition, Giacomini *et al.* (2008) had focussed not only on the Porto Vecchio - Fautea metasedimentary rock sequence, as in this study, but considered various rock types in the Porto Vecchio area including igneous rocks, to define a *P*-*T*-time path. According to our field study, we assume a tectonic boundary north of Punta di Fautea as the rocks there show significant migmatization, so that the higher temperatures, estimated by Giacomini *et al.* (2008) for the basement of Porto Vecchio could, indeed, be valid for this migmatized area. The granulites north of this area (granulites of Fautea-Solenzara) had experienced HP conditions at temperatures above 800°C before they joined the metamorphic evolution of the Porto Vecchio basement, i.e. they should have experienced the same P-T conditions as the rocks from the Porto Vecchio area (Giacomini *et al.*, 2008). The boundary of the Porto Vecchio-Fautea metasedimentary rock sequence to the south could be the PVSZ (Fig. 1b).

**Age constraints**

Typically, single monazite grains can contain different compositional domains providing information on the geological history of the host rock (Williams *et al.*, 2007). According to the different chemical compositions of monazite in the studied micaschists, three populations were distinguished (high, medium, and low Y) showing different ages (362, 351, 341 or 337 Ma depending on the rejection of possible outliers). It is not fully clear, if the medium-Y population results from the analysis of a mixture of high- and low-Y domains or represents a true discrete population, although the Y map of Figure 10c suggests three different Y domains. Because of this ambiguity, we discuss in the following the meaning of the high- and low-Y domains only. Monazite containing more than 2 wt% $Y_2O_3$ in metamorphic rocks usually formed before garnet, which competes with monazite for the trace contents of Y in a rock, or by strong retrogression of this phase (see, e.g., Massonne, 2014, 2016a). As our high-Y population is the oldest (~362 Ma) of the three ones in the micaschists, we suggest that it had formed before garnet started to grow. This is the case at pressures lower than 3 kbar (Fig. 9b) along the early prograde path. The preservation of monazite, formed already along such a path, might be rare but examples of preserved prograde monazite, which was even not shielded, for instance, as inclusion in garnet, exist in the literature (e.g., Langone *et al.*, 2011). Although zircon and monazite can give different ages in single rocks (Zeh *et al.*, 2003), a similar age of 361±3 Ma was obtained by Giacomini *et al.* (2008) from dating zircon in the Fautea-Solenzara granulites (see above). These authors assigned this Late Devonian age to the HP event of the granulites.

Some analyses of grains of the low-Y monazite population yielded Y contents even below the detection limit. We suggest that this population grew after garnet had grown and introduced the available Y. Another constraint for the relation of the age of the low-Y monazite population (~340 Ma) to the metamorphic evolution of the micaschists is the fact that the high-Y monazite was significantly corroded and replaced by low-Y monazite. This process can be deduced, for instance, from the elemental maps of the monazite of Figure 10. The high-Y domains in this grain survived only as relics. Even inner parts of this grain were replaced by the significantly younger low-Y domain. Thus, we assume that a deformational event or, more likely, the infiltration of hydrous fluids (see, e.g., Williams *et al.*, 2011; Lo Pò *et al.*, 2016) have caused the clear corrosion of high-Y monazite and its replacement by younger monazite. Such an event (deformation as reported above; fluid infiltration also resulted in partial replacement of sillimanite by micas) occurred close to peak *P*-*T* conditions after garnet had broadly grown. Even at very early retrograde conditions, an infiltration of hydrous fluids was noted leading to the corrosion of garnet. This process could have, in fact, released Y, but Y contents corresponding to up to 0.65 wt% $Y_2O_3$ were found in monazite of the low-Y population. Based on the above discussion, we think that the peak *P*-*T* conditions were reached at about 340 Ma or a bit earlier.

An age of 338±4 Ma was also obtained by Giacomini *et al.* (2008) as mean U-Pb concordia age of the youngest zircon population in a two-mica gneiss from the Punta di a Chiappa area. These authors related this age rather to the peak pressure of the metasedimentary rocks, but not to the peak temperature event, which was assumed to be somewhat younger (see Fig. 9c). The retrogression at still high temperatures was proposed by Giacomini *et al.* (2008) to have taken place mainly between 310 and 320 Ma (Fig. 9c). As such young monazite was not found in our micaschists, we doubt that these relatively young ages, obtained from igneous rocks (Giacomini *et al.*, 2008), are relevant for the early retrogression of the metamorphic rocks.

**Geodynamic scenario**

Giacomini *et al.* (2008) presented a geodynamic scenario for the evolution of the Corsica-Sardinia section of the Variscan orogen. This scenario is related to the collision of two continental plates, which started at about 360 Ma or somewhat earlier and led to continental subduction until the adhered oceanic crust was separated (slab break-off event). Giacomini *et al.* (2008) suggested these processes on the basis of the metamorphic evolution of the Fautea-Solenzara granulites deduced by these authors. The subsequent evolution, characterized by back-thrusting of slices from regions of thickened continental crust in major strike-slip shear zones in the time interval 350-315 Ma, is based on the *P*-*T*-time evolution derived from gneisses and migmatites of the Porto Vecchio area (Giacomini *et al.*, 2008). Our new findings on the studied micaschists from the Porto Vecchio-Fautea metasedimentary sequence, allow us to propose a modified collisional model.

In Figure 11, the evolution, exhibited in a two-dimensional scenario, starts with the final subduction of oceanic crust in Late Devonian times. The dehydration of the subducted crust has led to a magmatic arc which formed at the southern margin of Laurussia following, for instance, Rossi *et al*. (2009). The studied micaschists were situated in medium crustal depths (~12 km, see above) close to this arc at that time because this seems to be the most likely environment responsible for the high geothermal gradients (45-50 °C/km) which were deduced for the early evolution of the micaschists. The subsequent burial of these rocks to depths of 25 km was induced by the initial collision of Gondwana and Laurussia at the beginning of the Carboniferous (after formation of our high-Y monazite population at 362 Ma). At the same time, the magmatic arc became extinct because of the break-off of the oceanic plate which was adhered to Gondwana. In fact, this slab break-off process is assumed, by various authors to have taken place later (e.g., von Raumer *et al.*, 2014: 340-335 Ma; Casini *et al.*, 2015: 345-340 Ma with preference for 345 Ma), we think that no good evidence exists for the Variscan timing of this process yet.

In contrast to the micaschists, metamorphic rocks of the wider vicinity (those of NE Sardinia - see section GEOLOGICAL SETTING, General aspects) experienced HP conditions in the early Carboniferous as they were part of the downgoing continental plate and, thus, more deeply settled as the micaschists from the upper continental plate. However, both micaschists and HP rocks might have been more or less contemporaneously involved in back thrusting in an exhumation channel (for definition see, e.g., Massonne, 2016b) which comprises deeply buried sediments (e.g. HP micaschists reported by Cruciani *et al.*, 2013) and the adjacent uppermost portion of the downgoing plate and lowermost portion of the upper plate (see Fig. 11). This back-thrusting event, which might be typical for continent-continent collision settings (compare with the Himalayas: e.g. Catlos *et al.*, 2001; Iaccarino *et al.*, 2015; Carosi *et al.*, 2017), could have started after significant thrusting of the Gondwana margin under Laurussia (around 345 Ma). This event resulted in exhumation of the micaschists accompanied by cooling and penetration of hydrous fluids (at about 340 Ma according to the low-Y monazite population) because the sediments in the exhumation channel and the underlying upper portion of the downgoing plate, which were still relatively cold, were heated and, thus, dehydrated. These rocks experienced *P-T* conditions along a clockwise loop (see, e.g., Cruciani *et al.*, 2013) whereas the studied micaschists were metamorphosed along an anti-clockwise *P-T* path. Due to the back-thrusting event, rock slices from different crustal levels of both upper and lower continental plates were brought relatively close together probably still in Viséan times.

Shearing probably along strike-slip faults (see Giacomini *et al.*, 2008), which cannot be demonstrated in our two-dimensional model (Fig. 11), affected the Porto Vecchio basement including the studied micaschists (see above). According to our geodynamic model this tectonic event has already taken place in early Carboniferous times during the early exhumation of the studied micaschists. Casini *et al.* (2015) assumed that such an event in the Corsica-Sardinia block in the time interval 325-300 Ma has caused the production of large volumes of granitic melts forming extended batholiths in the Inner Zone of this block. This time interval is consistent with a major phase of transpression coeval with the development of lithospheric-scale shear zones between about 320 and 305 Ma (Di Vincenzo *et al.*, 2004; Carosi *et al.*, 2012). The contrasting time intervals are probably related to an apparent difference because compressional shearing seems to have occurred over a long period of time eventually during the entire Variscan orogeny.

## CONCLUSIONS

The study of a single rock sequence, characterized by similar metamorphic rock types (here metasediments), is worthwhile because it results in deeper insights into the evolution of crust during an orogenic event compared to the overall consideration of a crustal section which could not be as coherent as assumed. Occasionally, such a study reveals an anti-clockwise P-T loop (e.g., Pitra & Guiraud, 1996; Waizenhöfer & Massonne, 2017). This is the case for the here investigated micaschist-paragneiss sequence in the Corsican Porto Vecchio basement, which, in contrast to the previous study by Giacomini *et al.* (2008), experienced peak *P-T* conditions of 7 kbar at 600-630 °C. The prograde path of these rocks passed through relatively high temperatures (close to 600°C) at low pressures (around 4 kbar). The *P-T* evolution of the micaschist-paragneiss sequence, which might be bounded by strike-slip faults (in the south by the PVSZ), is explained by a geotectonic scenario related to the Variscan orogenesis (Fig. 11). This sequence experienced the high temperature - low pressure metamorphism close to a magmatic arc at c. 362 Ma according to the here presented monazite ages. The burial of this unit to depths of 25 km was initiated by continent-continent collision. The subsequent exhumation is hypothesized to have been accomplished by back-thrusting of continental slices in an exhumation channel.

## ACKNOWLEDGEMENTS

The authors thank Thomas Theye (Stuttgart) for his support of the work with the EMP. Sampling was carried out during a short-term visit of H.-J.M. at Università degli Studi di Cagliari funded by the visiting professor programme. M.F. and G.C. benefited from funds granted by Università degli Studi di Cagliari.

## REFERENCES

Bernhardt, H.-J., 2007. MINCALC-V5, a software tool for mineral analyses data processing. *Acta Microscopica*, **16**, 1-2, (Suppl. 2), 43.

Brandelik, A., 2009. CALCMIN – an EXCEL™ Visual Basic application for calculating mineral structural formulae from electron microprobe analyses. *Computers & Geosciences*, **35**, 1540-1551.

Carmignani, L., Carosi, R., Di Pisa, A., Gattiglio, M., Musumeci, G., Oggiano, G. & Pertusati, P. C., 1994. The Hercynian chain in Sardinia (Italy). *Geodinamica Acta* **7**, 31–47.

Carmignani, L., Oggiano, G., Barca, S., Conti, P., Eltrudis, A., Funedda, A., Pasci, S. &

Salvadori, I., 2001. Geologia della Sardegna (Note illustrative della Carta Geologica della Sardegna in scala 1:200000). Memorie descrittive della Carta Geologica d'Italia, Vol. LX, Servizio Geologico Nazionale. Istituto Poligrafico e Zecca dello Stato, Roma, 283 pp.

Carosi, R., Montomoli, C., Tiepolo, M. & Frassi, C., 2012. Geochronological constraints on post-collisional shear zones in the Variscides of Sardinia (Italy). *Terra Nova*, **24**, 42-51.

Carosi, R., Montomoli, C., Iaccarino, S., Massonne, H.-J., Rubatto, D., Langone, A., Gemignani, L. & Visonà, D., 2017. Middle to late Eocene exhumation of the Greater Himalayan Sequence in the Central Himalayas: Progressive accretion from the Indian plate. *Geological Society of America Bulletin*, **128**, 1571-1592.

Carosi, R. & Oggiano, G., 2002. Transpressional deformation in northwestern Sardinia (Italy): insights on the tectonic evolution of the Variscan Belt. *Comptes Rendus Geoscience*, **334**, 287-294.

Carosi, R. & Palmeri, R., 2002. Orogen-parallel tectonic transport in the Variscan belt of northeastern Sardinia (Italy): implications for the exhumation of medium-pressure metamorphic rocks. *Geological Magazine*, **139**, 497-511.

Casini, L., Cuccuru, S., Puccini, A., Oggiano, G. & Rossi, P., 2015. Evolution of the Corsica–Sardinia Batholith and late-orogenic shearing of the Variscides. Tectonophysics, 646, 65-78.

Catlos, E.J., Harrison, T.M., Kohn, M.J., Grove, M., Ryerson, F.J., Manning, C.E. & Upreti, B.N., 2001. Geochronologic and thermobarometric constraints on the evolution of the Main Central Thrust, central Nepal Himalaya. *Journal of Geophysical Research*, **106**, 16177-16204.

Connolly, J.A.D., 2005. Computation of phase equilibria by linear programming: a tool for geodynamic modeling and its application to subduction zone decarbonation. *Earth and*

*Planetary Science Letters*, **236**, 524-541.

Cortesogno, L., Gaggero, L., Oggiano, G. & Paquette, J.-L., 2004. Different tectono-thermal evolutionary paths in eclogitic rocks from the axial zone of the Variscan chain in Sardinia (Italy) compared with the Ligurian Alps. *Ofioliti*, **29**, 125–144.

Cruciani, G., Franceschelli, M., Elter, F. M., Puxeddu, M. & Utzeri, D., 2008a. Petrogenesis of Al-silicate-bearing trondhjemitic migmatites from NE Sardinia, Italy: *Lithos*, **102**, 554-574.

Cruciani, G., Franceschelli, M., Jung, S., Puxeddu, M. & Utzeri, D., 2008b. Amphibole-bearing migmatites from the Variscan Belt of NE Sardinia, Italy: Partial melting of mid-Ordovician igneous sources: *Lithos*, **105**, 208-224.

Cruciani, G., Franceschelli, M. & Groppo, C., 2011. P-T evolution of eclogite-facies metabasite from NE Sardinia, Italy: insights into the prograde evolution of Variscan eclogites. *Lithos*, **121**, 135-150.

Cruciani, G., Franceschelli, M., Groppo, C. & Spano, M.E., 2012. Metamorphic evolution of non-equilibrated granulitized eclogite from Punta de li Tulchi (Variscan Sardinia) determined through texturally controlled thermodynamic modelling. *Journal of Metamorphic Geology*, **30**, 667-685.

Cruciani, G., Franceschelli, M., Massonne, H.-J., Carosi, R. & Montomoli, C., 2013. Pressure-temperature and deformational evolution of high-pressure metapelites from Variscan NE Sardinia, Italy. *Lithos*, **175-176**, 272-284.

Cruciani, G., Franceschelli, M., Groppo, C., Oggiano, G. & Spano, M.E. 2015. Re-equilibration history and P-T path of eclogites from Variscan Sardinia, Italy: a case study from the medium-grade metamorphic complex. *International Journal of Earth Sciences*, **104**, 797-814.

Cruciani, G., Franceschelli, M., Massonne, H.-J., Musumeci, G. & Spano, M. E., 2016. Thermomechanical evolution of the high-grade core in the nappe zone of Variscan

Sardinia, Italy: the role of shear deformation and granite emplacement. *Journal of metamorphic Geology*, **34**, 321-342.

Di Vincenzo, G., Carosi, R. & Palmeri, R., 2004. The Relationship between tectono-metamorphic evolution and argon isotope records in white mica: constraints from *in situ* $^{40}Ar$–$^{39}Ar$ laser analysis of the Variscan basement of Sardinia. *Journal of Petrology*, **45**, 1013-1043.

Elter, F.M., Musumeci, G. & Pertusati, P.C., 1990. Late Hercynian shear zones in Sardinia. *Tectonophysics*, **176**, 387–404.

Elter, F.M., Faure, M., Ghezzo, C. & Corsi, B., 1999. Late Hercynian shear zones in northeastern Sardinia (Italy): Géologie de la France, **2**, 3-16.

Faure, M., Rossi, P., Gaché, J., Melleton, J., Frei, D., Li, X. & Lin, W., 2014. Variscan orogeny in Corsica: new structural and geochronological insights, and its place in the Variscan geodynamic framework. *International Journal of Earth Sciences,* **103**, 1533-1551.

Franceschelli, M., Puxeddu, M., Cruciani, G. & Utzeri D., 2007. Metabasites with eclogite facies relics from Variscides in Sardinia, Italy: a review. *International Journal of Earth Sciences*, **96**, 795-815.

Fuhrman, M.L. & Lindsley, D.H., 1988. Ternary-feldspar modeling and thermometry. *American Mineralogist*, **73**, 201-215.

Ghezzo, C. & Orsini, J.-B., 1982. Lineamenti strutturali e composizionali del batolite ercinico Sardo-Corso in Sardegna. In: Carmignani, L., Cocozza, T., Ghezzo, C., Pertusati, P. C. & Ricci C. A. (eds.) Guida alia geologia del Paleozoico sardo. Guide geologiche regionali. Memorie della Società Geologica Italiana, 165-181.

Giacomini, F., Bomparola, R.M. & Ghezzo, C., 2005. Petrology and geochronology of metabasites with eclogite facies relics from NE Sardinia: constraints for the Palaeozoic evolution of Southern Europe. *Lithos*, **82**, 221–248.

Giacomini, F., Dallai, L., Carminati, E., Tiepolo, M. & Ghezzo, C., 2008. Exhumation of a Variscan orogenic complex: insights into the composite granulitic–amphibolitic metamorphic basement of south-east Corsica (France). *Journal of Metamorphic Geology*, **26**, 403-436.

Groppo, C. & Rolfo, F. 2008. Counterclockwise P-T evolution of the Aghil Range: Metamorphic record of an accretionary melange between Kunlun and Karakorum (SW Sinkiang, China). *Lithos*, **105**, 365-378.

Holland, T. & Powell, R., 1996. Thermodynamics of order-disorder in minerals: II. Symmetric formalism applied to solid solutions. *American Mineralogist*, **81**, 1425-1437.

Holland, T.J.B. & Powell, R., 1998. An internally consistent thermodynamic data set for phases of petrological interest. *Journal of Metamorphic Geology*, **16**, 309-343.

Holland, T., Baker, J. & Powell, R., 1998. Mixing properties and activity-composition relationships of chlorites in the system $MgO$-$FeO$-$Al_2O_3$-$SiO_2$-$H_2O$. *European Journal of Mineralogy*, **10**, 395-406.

Iaccarino, S., Montomoli, C., Carosi, R., Massonne, H.-J., Langone, A. & Visonà, D., 2015. Pressure-temperature-time-deformation path of kyanite-bearing migmatitic paragneiss in the Kali Gandaki valley (Central Nepal): Investigation of Late Eocene-Early Oligocene melting processes. *Lithos*, **231**, 103-121.

Iacopini, D., Carosi, R., Montomoli, C. & Passchier, C. W., 2008. Strain analysis and vorticity of flow in the northern Sardinian Variscan belt: recognition of a partitioned oblique deformation event. *Tectonophysics*, **446**, 77–96.

Jeřábek, P., Janák, M., Faryad, S.W., Finger, F. & Konečný, P., 2008. Polymetamorphic evolution of pelitic schists and evidence for Permian low-pressure metamorphism in the Vepor Unit, West Carpathians. *Journal of Metamorphic Geology*, **26**, 465-485.

Langone, A., Braga, R., Massonne, H.-J. & Tiepolo, M., 2011. Preservation of old (prograde metamorphic) U-Th-Pb ages in unshielded monazite from the high-pressure paragneisses of the Variscan Ulten Zone (Italy). *Lithos*, **127**, 68-85.

Liu, Y., Siebel, W., Theye, T. & Massonne, H.-J., 2011. Isotopic and structural constraints on the late Miocene to Pliocene evolution of the Namche Barwa area, eastern Himalayan syntaxis, SE Tibet. *Gondwana Research*, **19**, 894-909.

Lo Pò, D., Braga, R., Massonne, H.-J., Molli, G., Montanini, A. & Theye, T., 2016. Fluid-induced breakdown of monazite in medium-grade metasedimentary rocks of the Pontremoli basement (Northern Apennines, Italy). *Journal of Metamorphic Geology*, **34**, 63-84.

Ludwig, K. R., 1999. Isoplot/Ex, Version 2.06: A Geochronological Tool-kit for Microsoft Excel. 1a. Berkeley Geochronology Center, *Special Publications*, pp. 1-49.

Massonne, H.-J., 2010. Phase relations and dehydration behaviour of calcareous sediments at very-low to low grade metamorphic conditions. *Periodico di Mineralogia*, **79**, 21-43.

Massonne, H.-J., 2012. Formation of amphibole and clinozoisite-epidote in eclogite owing to fluid infiltration during exhumation in a subduction channel. *Journal of Petrology*, **53**, 1969-1998.

Massonne, H.-J., 2014. Wealth of P–T–t information in medium-high grade metapelites: Example from the Jubrique Unit of the Betic Cordillera, S Spain. *Lithos*, **208-209**, 137-157.

Massonne, H.-J., 2016a. Tertiary high-pressure metamorphism recorded in andalusite-bearing mica-schist, southern Pirin Mts., SW Bulgaria. *European Journal of Mineralogy*, in press. doi: 10.1127/ejm/2016/0028-2575.

Massonne, H.-J., 2016b. Hydration of the lithospheric mantle by the descending plate in a continent–continent collisional setting and its geodynamic consequences. *Journal of Geodynamics*, **96**, 50-61.

Massonne, H.-J. & Schreyer, W., 1986. High-pressure syntheses and X-ray properties of white micas in the system $K_2O$-MgO-$Al_2O_3$-$SiO_2$-$H_2O$. *Neues Jahrbuch für Mineralogie Abhandlungen*, **153**, 177-215.

Massonne, H.-J. & Toulkeridis, T., 2012. Widespread relics of high-pressure metamorphism confirm major terrane accretion in Ecuador: a new example from the Northern Andes. *International Geology Review*, **54**, 67-80.

Massonne, H.-J. & Willner, A.P., 2008. Dehydration behaviour of metapelites and mid-ocean ridge basalt at very-low to low grade metamorphic conditions. *European Journal of Mineralogy*, **20**, 867-879.

Massonne, H.-J., Dristas, J.A. & Martínez, J.C., 2012. Metamorphic evolution of the Río de la Plata craton in the Cinco Cerros area, Buenos Aires Province, Argentina. *Journal of South American Earth Sciences*, **38**, 57-70.

Massonne, H.-J., Cruciani, G. & Franceschelli, M., 2013. Geothermobarometry on anatectic melts - a high-pressure Variscan migmatite from northeast Sardinia. *International Geology Review*, **55**, 1490-1505.

Ménot, R. P. & Orsini, J. B., 1990. Evolution du socle anté-stephanien de Corse: événements magmatiques et métamorphiques. *Schweizerische Mineralogische und Petrographische Mitteilungen,* **70**, 35-53.

Palmeri, R., Fanning, M., Franceschelli, M., Memmi, I. & Ricci, C. A., 2004. SHRIMP dating of zircons in eclogite from the Variscan basement in north-eastern Sardinia (Italy). *Neues Jahrbuch für Mineralogie Monatshefte*, **6**, 275–288.

Paquette, J.-L., Ménot, R.-P., Pin, C. & Orsini, J.-B., 2003. Episodic and short-lived granitic pulses in a post-collisional setting: evidence from precise U-Pb zircon dating through a crustal cross-section in Corsica. *Chemical Geology*, **198**, 1-20.

Pitra, P. & Guiraud, M., 1996. Probable anticlockwise P-T evolution in extending crust: Hlinsko region, Bohemian Massif. *Journal of Metamorphic Geology*, **14**, 49-60.

Powell, R. & Holland, T., 1999. Relating formulations of the thermodynamics of mineral solid solutions: Activity modeling of pyroxenes, amphiboles, and micas. *American Mineralogist*, **84**, 1-14.

Rossi, P. & Cocherie, A., 1991. Genesis of a Variscan batholith: field, petrological and mineralogical evidence from the Corsica-Sardinia batholith. *Tectonophysics*, **195**, 319–346.

Rossi, P., Oggiano, G.& Cocherie, A., 2009. A restored section of the "southern Variscan realm" across the Corsica-Sardinia microcontinent. *Comptes Rendus Géoscience*, **341**, 224-238.

Rouire, J., Rossi, P., Bourges, F., Libourel, G. & Dominici, R. 1993. Carte Géologique de la France (1 ⁄ 50000), feuille Porto- Vecchio (1124). Notice explicative par Rouire, J., Rossi, P., Bourge, F., Libourel, G. & Dominici, G., pp. 63. BRGM,Orleans. ISBN 2-7159-2124-1.

von Raumer, J.F., Finger, F., Vesel, P. & Stampfli, G.M., 2014. Durbachites–Vaugnerites – a geodynamic marker in the central European Variscan orogen. *Terra Nova*, **26**, 85-95.

Waizenhöfer, F. & Massonne, H.-J., 2017. Monazite in a Variscan mylonitic paragneiss from the Münchberg Metamorphic Complex (NE Bavaria) records Cadomian protolith ages. *Journal of Metamorphic Geology*, in press. doi:10.1111/jmg.12240.

Wang, J.M., Zhang, J.J. & Wang, X.X., 2013. Structural kinematics, metamorphic P–T profiles and zircon geochronology across the Greater Himalayan Crystalline Complex in south-central Tibet: implication for a revised channel flow: *Journal of Metamorphic Geology*, **31**, 607–628.

Williams, M.L., Jercinovic, M.J. & Hetherington, C.J., 2007. Microprobe monazite geochronology: understanding geologic processes by integrating composition and chronology. *Annual Review of Earth and Planetary Sciences*, **35**, 137-175.

Williams, M.L., Jercinovic, M.J., Harlov, D.E., Budzyń, B. & Hetherington, C.J., 2011. Resetting monazite ages during fluid-related alteration. *Chemical Geology*, **283**, 218-

225.

Zeh, A., Williams, I.S., Brätz, H. & Millar, I.L., 2003. Different age response of zircon and monazite during the tectono-metamorphic evolution of a high grade paragneiss from the Ruhla Crystalline Complex, central Germany. *Contributions to Mineralogy and Petrology*, **145**, 691-706.

Zeh, A., Holland, T.J.B. & Klemd, R., 2005. Phase relationships in grunerite–garnet-bearing amphibolites in the system CFMASH, with applications to metamorphic rocks from the Central Zone of the Limpopo Belt, South Africa. *Journal of Metamorphic Geology*, **23**, 1-17.

Zhou, H.-W. & Murphy, M.A., 2005. Tomographic evidence for wholesale underthrusting of India beneath the entire Tibetan plateau. *Journal of Asian Earth Sciences*, **25**, 445-457.

## Figure Captions

**Fig. 1. (a)** Geological overview map of Corsica slightly modified after Faure *et al.* (2014). **(b)** Detailed geological map of the area where micaschist sample Cors15G was taken. This map around the Porto Vecchio shear zone (PVSZ) was simplified after Rouire *et al.* (1993) and Giacomini *et al.* (2008). The stereographic projection of structural elements is related to measurements undertaken by the authors: green dots = metamorphic foliation, red dots = mylonitic foliation, blue triangles = mylonitic lineations.

**Fig. 2. (a)** Geological sketch map of the area at Punta di Fautea; **(b)** Intensely foliated medium-coarse grained micaschists and paragneisses near Punta di Fautea. The main metamorphic foliation is deformed by late assymetric folds. Length of photo: 25 cm. **(c)** White mica-bearing micaschist with cm-sized euhedral garnet near Punta di Fautea. Length of photo: 20 cm.

**Fig. 3.** Photomicrographs of objects in micaschist samples Cors15G **(a,b,e)** and Cors17 **(c,d,f)** seen under plane polarised light (left hand side of each image) and crossed polarisers (right hand side). Bt = biotite, Gt = garnet, Mu = muscovite, Pl = plagioclase, Q = quartz, Si = sillimanite. The image widths are 4 mm (a-d) or 0.5 mm. **(a)** Older mm-sized white-mica grains surrounded by the finer-grained younger mica generation. **(b)** Pinite-like pseudomorph after garnet. Several small relics of garnet are still present in this pseudomorph. **(c)** The left hand side of the image shows a mica-rich band with several bended and kinked mica grains of the older mica generation. The upper right portion of the image is part of a quartz-feldspar band. **(d)** A small garnet grain in contact with a mm-sized plagioclase blast which is surrounded by smaller plagioclase grains. **(e)** A cluster of sillimanite (fibrolite) enveloped by an aggregate of very fine-grained mica which is surrounded by coarser-grained muscovite. **(f)** All three generations of micas (see text) are in contact to each other.

**Fig. 4.** Elemental maps of a garnet (fragment) in micaschist **(a)** Cors15G and **(b)** Cors17 obtained with a CAMECA SX100 EMP. The scales for the colour code on the right hand side of each image indicate counts of specific X-ray radiation per time unit.

**Fig. 5.** Results of EMP analyses of garnet in micaschist Cors15G **(a)** and Cors17 **(b)** in terms of molar fractions of grossular (+ andradite) (XCa), pyrope (XMg), and spessartine (XMn). The solid lines show the chemical trends from the inner core to the outer mantle of garnet. The arrow of the broken line points to retrograde compositions analysed at the rim of garnet fragments formed after considerable corrosion.

**Fig. 6.** Elemental maps of mica clusters in micaschist **(a)** Cors15G and **(b)** Cors17 obtained with a CAMECA SX100 EMP. The scales for the colour code on the right hand side of each image indicate counts of specific X-ray radiation per time unit. Typically, large grains of the oldest mica generation are replaced by significantly finer grained micas of a later generation, which contain, for instance, lower Ti contents than the older, large grains. Abbreviations for minerals as in Figure 3.

**Fig. 7.** Results of EMP spot analyses of white mica in samples **(a)** Cors15G and **(b)** Cors17 in terms of Si contents (pdfu = per double formula unit) versus those of diverse cations (see legend). For further information see text.

**Fig. 8.** **(a)** Example for a *P*-*T* pseudosection calculated in this study with the computer software package PERPLE_X (see text). The displayed one is for the $Fe^{3+}$-free, $H_2O$-rich composition of sample Cors15G (Table 3). Abbreviations: Am = Na-rich amphibole, An = andalusite, Bt = biotite, Ch = chlorite, Co = cordierite, Gt = garnet, Im = ilmenite, Kf = K-

feldspar, Lw = lawsonite, Om = Na-rich clinopyroxene, Pa = paragonite, Ph = potassic white-mica, Pl = plagioclase, Q = quartz, Rt = rutile, Si = sillimanite, St = staurolite, Tt = titanite, Zo = zoisite. **(b, c)** Contouring of the *P-T* pseudosection shown in (a) by isopleths for molar fractions of the garnet components grossular (+ andradite), XCa, and pyrope, XMg, the modal content of garnet, Gt vol%, and the Si content (pdfu) in potassic white-mica. The bold curves mark the limits of the occurrence of garnet and potassic white-mica.

**Fig. 9. (a, b)** Estimates of *P-T* conditions (error ellipses) and paths (thick lines with arrow heads) using garnet and potassic white-mica isopleths (exemplarily shown in Fig. 8). The coloured lines refer to various kinds of isopleths (green: XMg = molar fraction of pyrope in garnet, red: XCa = molar fraction of grossular+andradite in garnet, light blue: XMn = molar fraction of spessartine in garnet; dark yellow: modal content of garnet, blue: Si content of potassic white mica). The black lines mark the *P-T* limits of various phases (for abbreviations see Fig. 8 and Mu = muscovite). The solid lines in (a) are related to the bulk-rock composition of Cors15G without $Fe^{3+}$ but corrected for Ca in apatite. The broken lines (except *P-T* path) and the labelling in italics in this graph refer to this composition with less $H_2O$ (semi-dry in Table 3). The solid lines and grey ellipses in (b) are related to the bulk-rock composition of Cors17 with 5% Fe being trivalent and no correction for Ca in apatite. The broken lines (except *P-T* path) in this graph refer to this composition but with a lower Ca content due to the apatite correction. The dashed-dotted lines and pink ellipses are related to Cors17 without $Fe^{3+}$ and apatite correction. The long axes of the ellipses mark the supposed largest error owing to P-T intersections of relevant isopleths considering a certain analytical error, for instance, in the garnet composition. **(c)** The solid P-T paths, which were also shown in (a) and (b), are constrained by chemically zoned garnet and other observations on micaschists Cors15G and Cors17. The broken P-T paths are less well constrained. The light grey path is that from Giacomini *et al.* (2008) for "the paragneisses from Porto Vecchio", which considers,

for instance, information from igneous rocks in the neighbourhood of the paragneisses as well. Thus, we generally relate this path to the basement east and north-east of Porto Vecchio.

**Fig. 10.** **(a)** Elemental map for Y in a monazite grain of micaschist Cors15G. Cold colours (blue) of the colour code mark lower counting rates than warm colours (red). **(b-d)** Unusual large monazite grain in Cors15G with significant zonation shown by a BSE image and elemental maps for Y and Ce. For colour coding see (a). **(e)** Critical chemical parameters (see legend and text) of monazite plotted versus age. Three groups were distinguished on the basis of these parameters. The arbitrarily chosen limits are at Y contents of 6.5 and 20.3 ($Y_2O_3$/0.1 wt.%). Not shown are 2 data for the Th/U ratio which amount to 76.2 (age: 367.8 Ma) and 71.4 (353.6 Ma). For the given mean ages and their errors see text.

**Fig. 11.** Two-dimensional continent-continent collisional scenario, similar to that suggested by Massonne (2016b). **(a)** It considers the subduction of an oceanic plate between continental plates, with a contemporaneous supply of magmas to allow for the perpetual existence of a magmatic arc. **(b)** Soon after the beginning of the continent-continent collision a slab break-off process occurs. **(c,d)** The subsequent process is characterized by progressive thickening of continental crust leading to an extended area of thick continental crust. The exhibited scenario is related to colliding Gondwana and Laurussia in the region of the Corsica-Sardinia block. Markers (blue and yellow) represent volumes of rocks which are now exposed in the Porto Veccchio area (micaschist-paragneiss sequence) and in NE Sardinia (HP migmatites). The suggested timing is based on the here presented monazite ages. For further details see text.

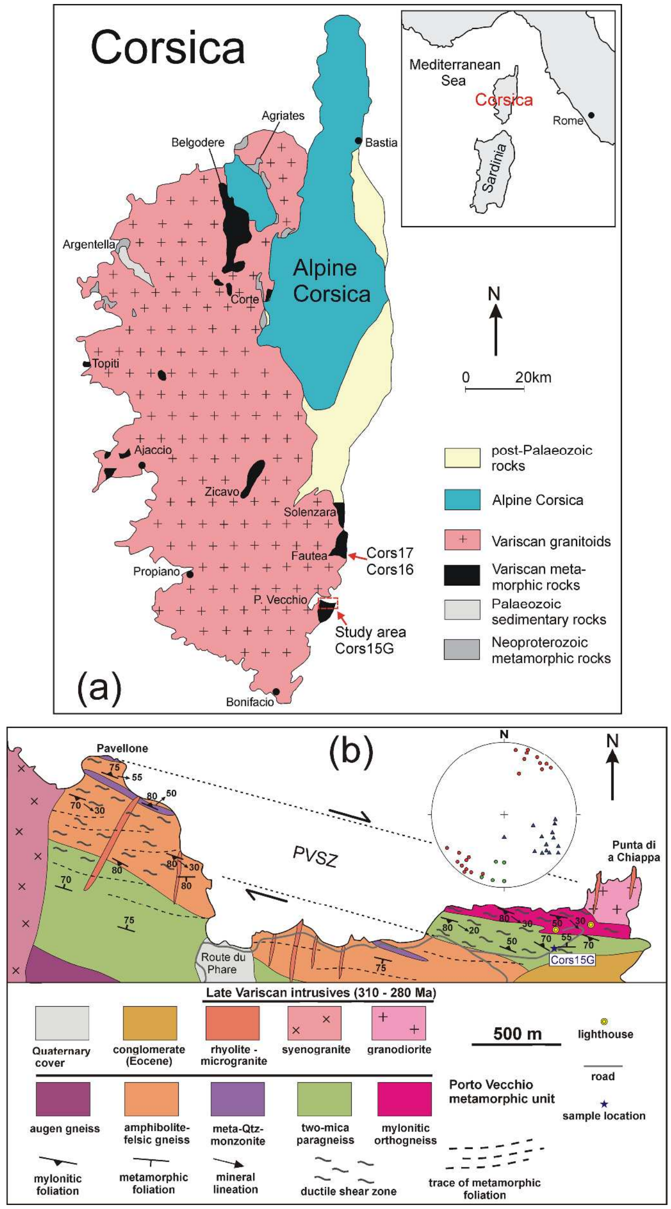
Corsica
Mediterranean Sea
Corsica
Rome
Sardinia
Agriates
Belgodere
Bastia
Argentella
Alpine Corsica
Corte
N
0 20km
Topiti
Ajaccio
Zicavo
Solenzara
Fautea
Cors17
Cors16
Propiano
P. Vecchio
Study area
Cors15G
Bonifacio
(a)
post-Palaeozoic rocks
Alpine Corsica
Variscan granitoids
Variscan meta-morphic rocks
Palaeozoic sedimentary rocks
Neoproterozoic metamorphic rocks
(b)
Pavellone
PVSZ
Punta di a Chiappa
Route du Phare
Cors15G
Late Variscan intrusives (310 - 280 Ma)
Quaternary cover
conglomerate (Eocene)
rhyolite - microgranite
syenogranite
granodiorite
500 m
lighthouse
road
Porto Vecchio metamorphic unit
sample location
augen gneiss
amphibolite-felsic gneiss
meta-Qtz-monzonite
two-mica paragneiss
mylonitic orthogneiss
mylonitic foliation
metamorphic foliation
mineral lineation
ductile shear zone
trace of metamorphic foliation

Figure 1

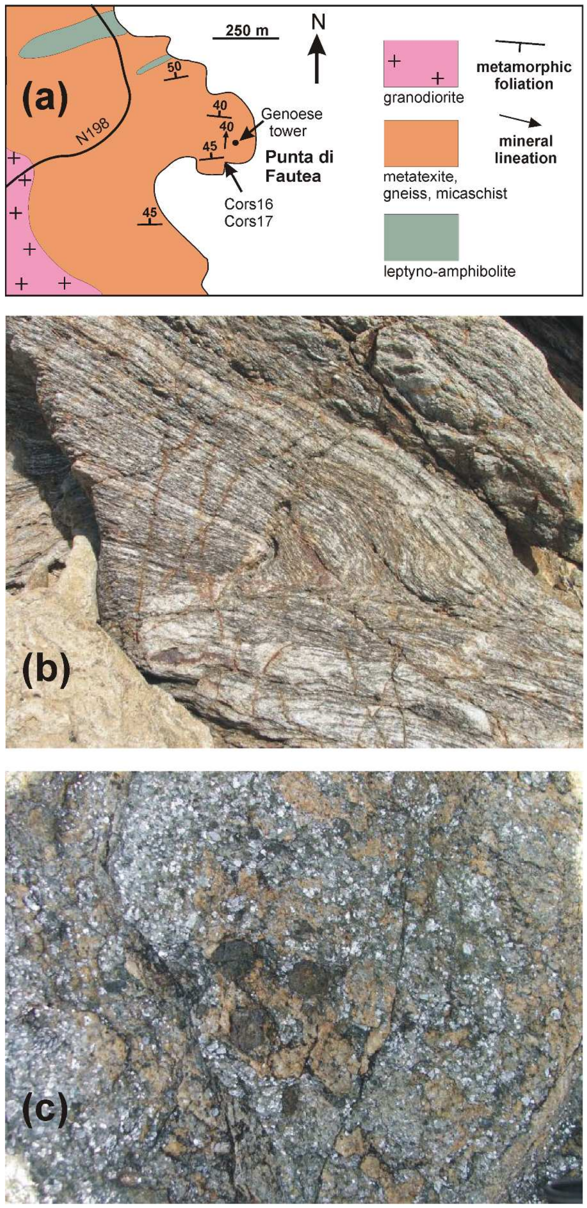
(a)
250 m
N
50
40
40
45
45
N198
Genoese tower
Punta di Fautea
Cors16
Cors17
granodiorite
metamorphic foliation
mineral lineation
metatexite, gneiss, micaschist
leptyno-amphibolite
(b)
(c)

Figure 2

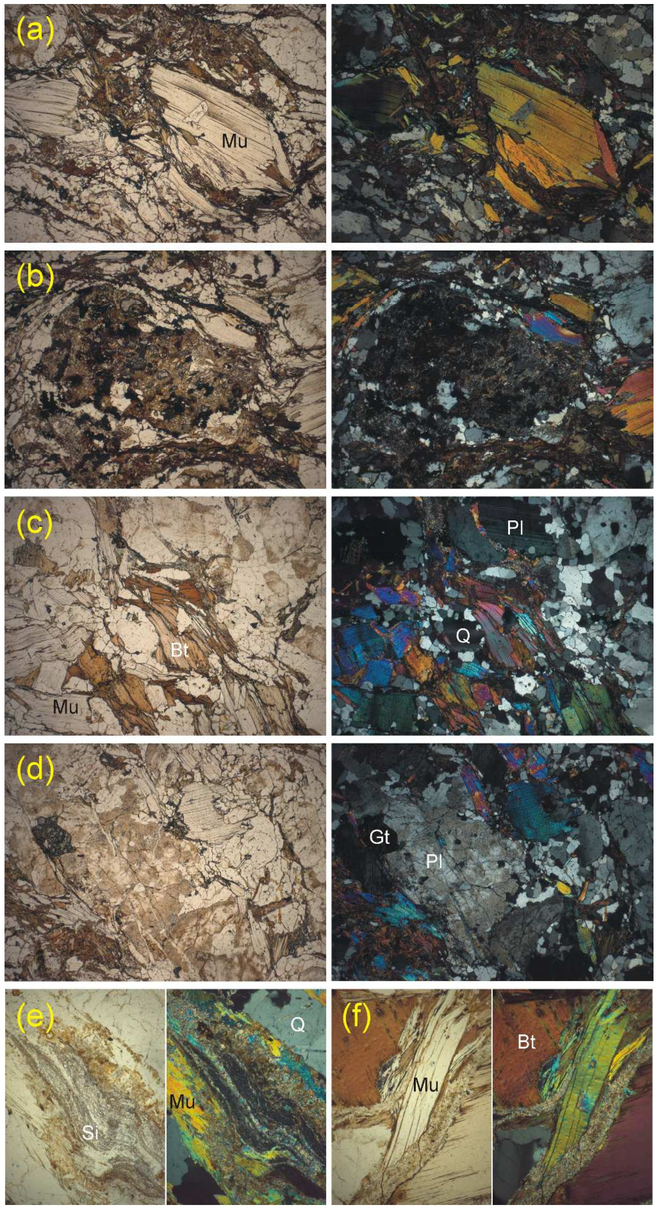


Figure 3

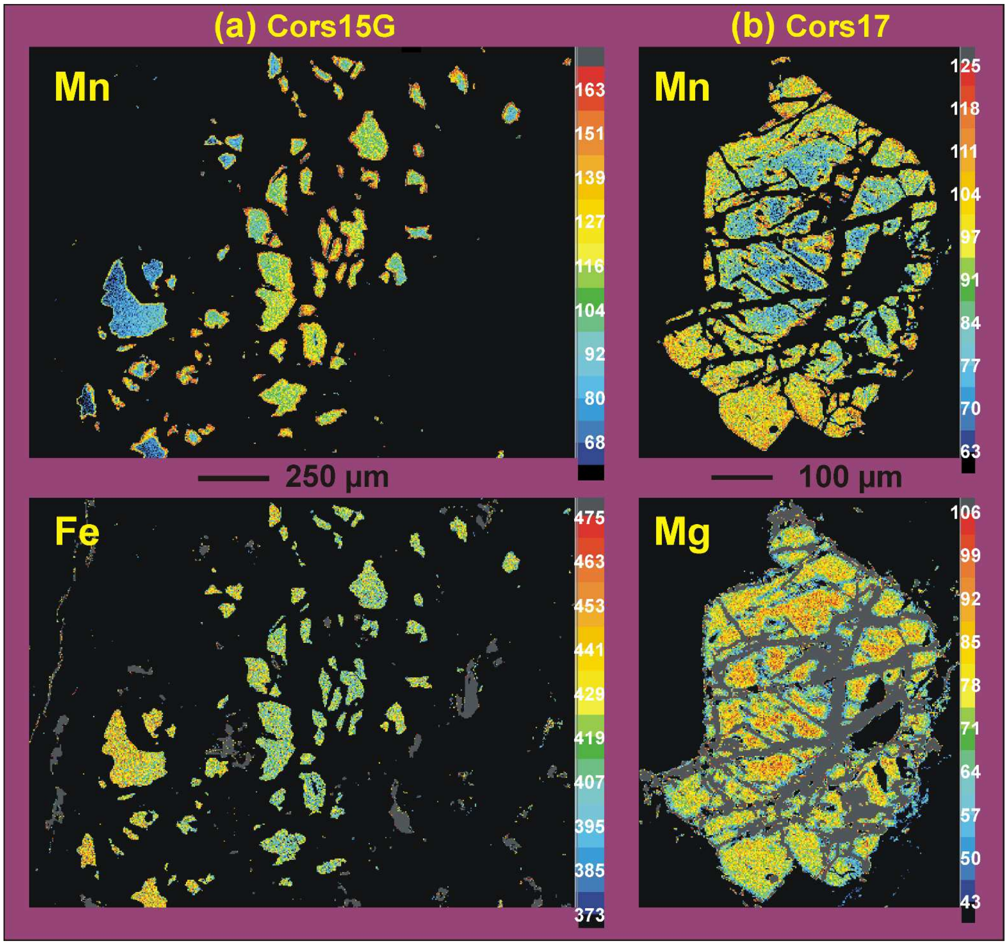
(a) Cors15G
(b) Cors17
Mn
163
151
139
127
116
104
92
80
68
Mn
125
118
111
104
97
91
84
77
70
63
250 µm
100 µm
Fe
475
463
453
441
429
419
407
395
385
373
Mg
106
99
92
85
78
71
64
57
50
43

Figure 4

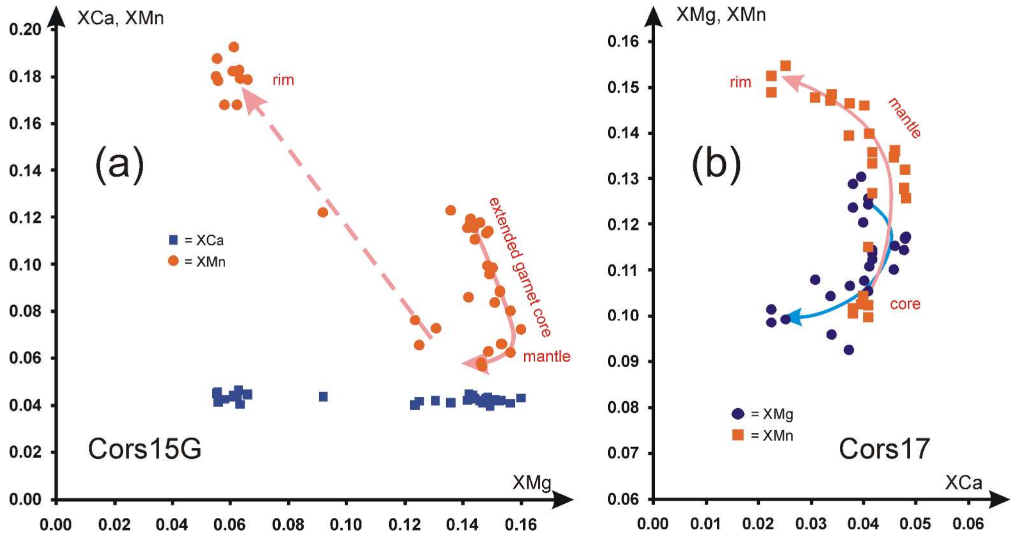
XCa, XMn
(a)
= XCa
= XMn
rim
extended garnet core
mantle
Cors15G
XMg
0.20
0.18
0.16
0.14
0.12
0.10
0.08
0.06
0.04
0.02
0.00
0.00
0.02
0.04
0.06
0.08
0.10
0.12
0.14
0.16
XMg, XMn
(b)
rim
mantle
core
= XMg
= XMn
Cors17
XCa
0.16
0.15
0.14
0.13
0.12
0.11
0.10
0.09
0.08
0.07
0.06
0.00
0.01
0.02
0.03
0.04
0.05
0.06

Figure 5

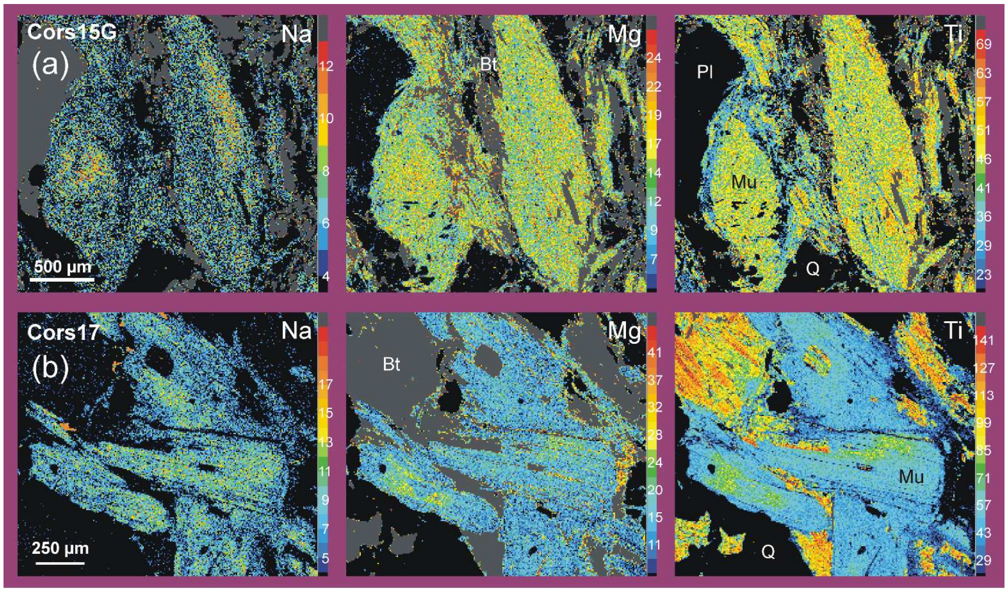
Cors15G
(a)
Na
Mg
Ti
Bt
Pl
Mu
Q
500 µm
12
10
8
6
4
24
22
19
17
14
12
9
7
69
63
57
51
46
41
36
29
23
Cors17
(b)
Na
Mg
Ti
Bt
Mu
Q
250 µm
17
15
13
11
9
7
5
41
37
32
28
24
20
15
11
141
127
113
99
85
71
57
43
29

Figure 6

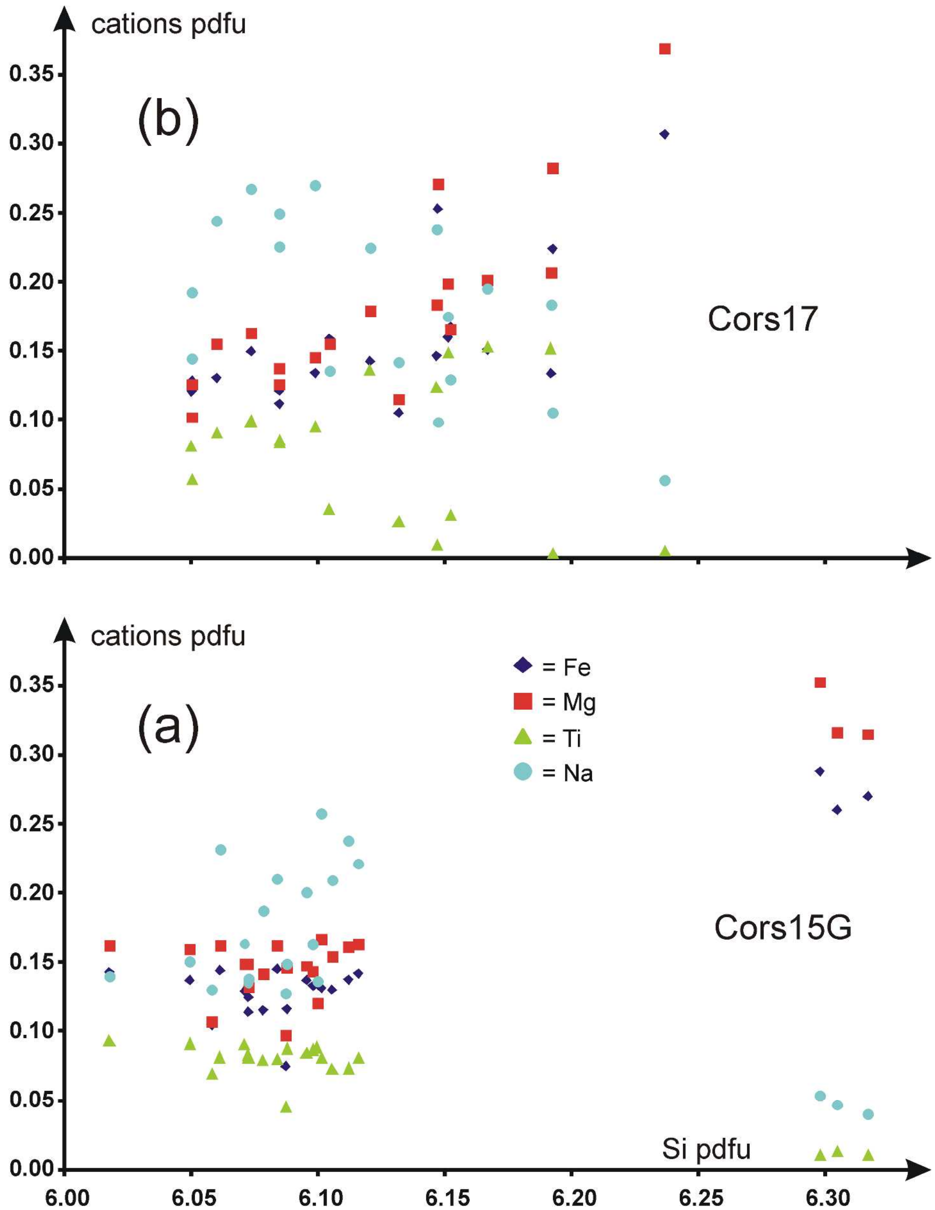
cations pdfu
0.35
0.30
0.25
0.20
0.15
0.10
0.05
0.00
(b)
Cors17
cations pdfu
= Fe
= Mg
= Ti
= Na
(a)
Cors15G
Si pdfu
6.00
6.05
6.10
6.15
6.20
6.25
6.30

Figure 7

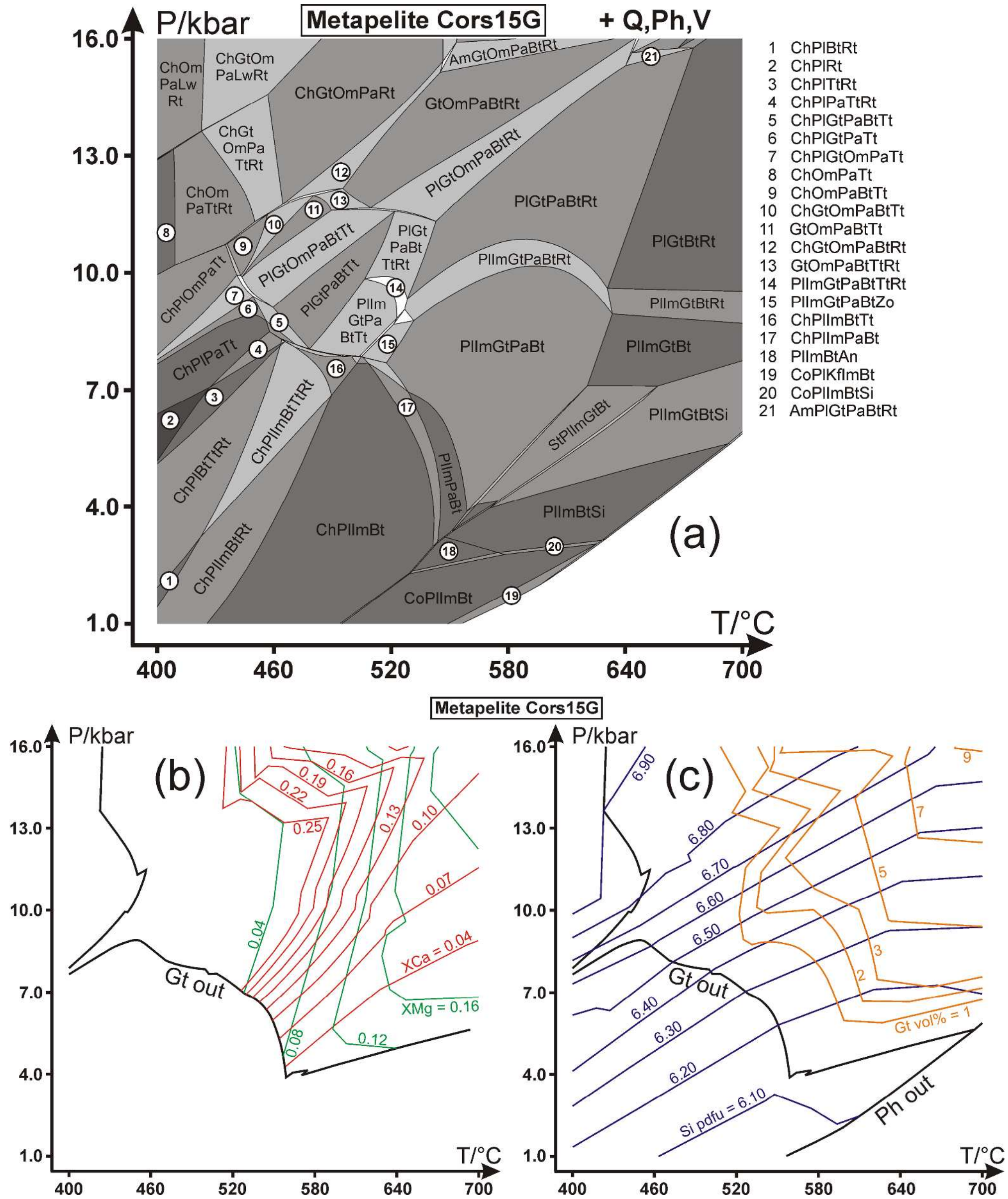

Metapelite Cors15G
+ Q,Ph,V
P/kbar
T/°C
(a)
1 ChPlBtRt
2 ChPlRt
3 ChPlTtRt
4 ChPlPaTtRt
5 ChPlGtPaBtTt
6 ChPlGtPaTt
7 ChPlGtOmPaTt
8 ChOmPaTt
9 ChOmPaBtTt
10 ChGtOmPaBtTt
11 GtOmPaBtTt
12 ChGtOmPaBtRt
13 GtOmPaBtTtRt
14 PlImGtPaBtTtRt
15 PlImGtPaBtZo
16 ChPlImBtTt
17 ChPlImPaBt
18 PlImBtAn
19 CoPlKfImBt
20 CoPlImBtSi
21 AmPlGtPaBtRt
Metapelite Cors15G
(b)
Gt out
XCa = 0.04
XMg = 0.16
(c)
Gt out
Ph out
Si pdfu = 6.10
Gt vol% = 1


Figure 8

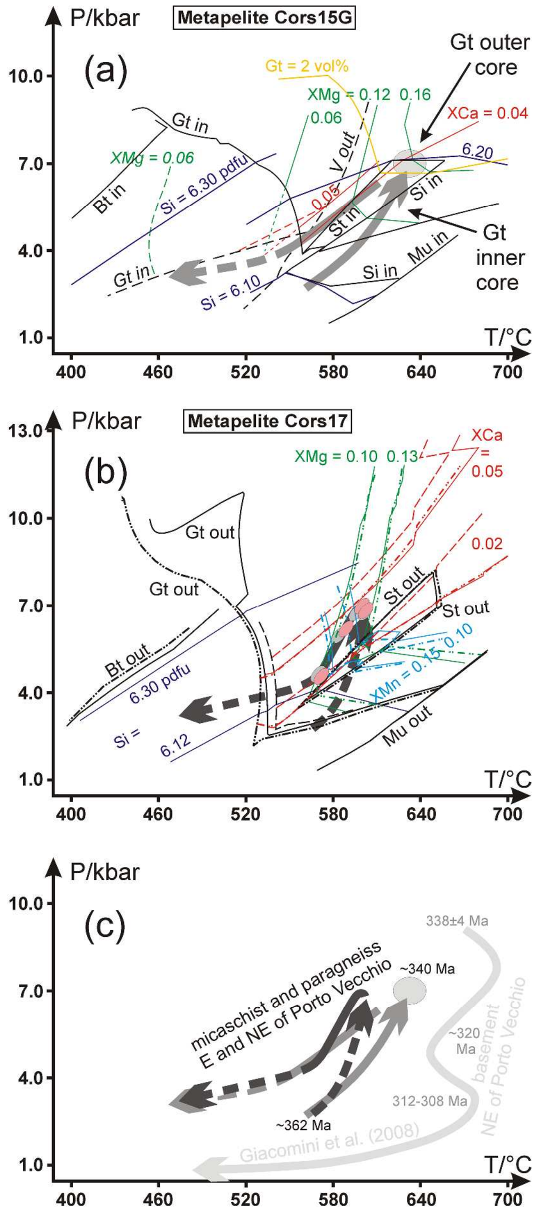

P/kbar
Metapelite Cors15G
(a)
Gt outer core
Gt = 2 vol%
XMg = 0.12
0.16
XCa = 0.04
0.06
Gt in
V out
XMg = 0.06
Si = 6.30 pdfu
6.20
Bt in
0.05
St in
Si in
Gt inner core
Mu in
Si in
Gt in
Si = 6.10
T/°C
P/kbar
Metapelite Cors17
(b)
XCa = 0.05
XMg = 0.10
0.13
Gt out
Gt out
0.02
St out
St out
Bt out
6.30 pdfu
XMn = 0.15
0.10
Si =
6.12
Mu out
T/°C
P/kbar
(c)
338±4 Ma
micaschist and paragneiss E and NE of Porto Vecchio
~340 Ma
~320 Ma
basement NE of Porto Vecchio
312-308 Ma
~362 Ma
Giacomini et al. (2008)
T/°C


Figure 9

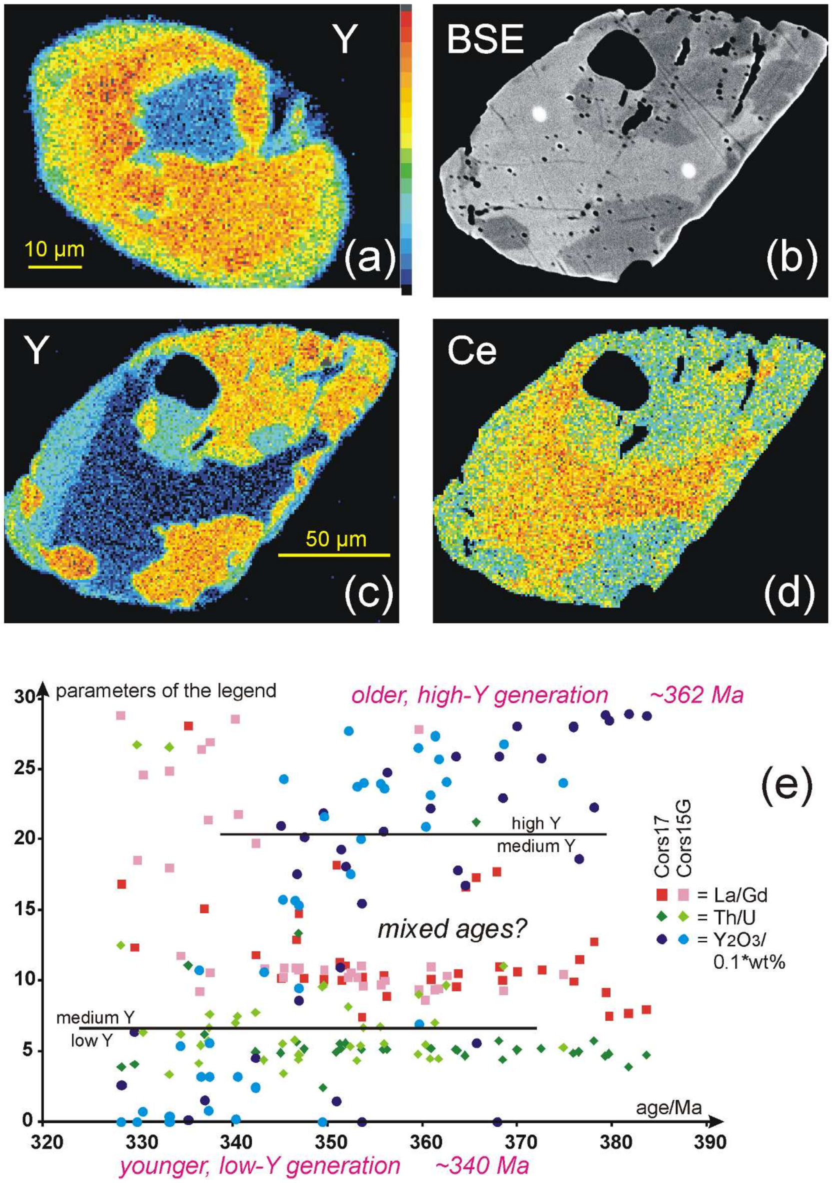
Y
10 µm
(a)
BSE
(b)
Y
50 µm
(c)
Ce
(d)
parameters of the legend
older, high-Y generation ~362 Ma
(e)
high Y
medium Y
mixed ages?
medium Y
low Y
Cors17
Cors15G
= La/Gd
= Th/U
= Y2O3/ 0.1*wt%
age/Ma
younger, low-Y generation ~340 Ma

Figure 10

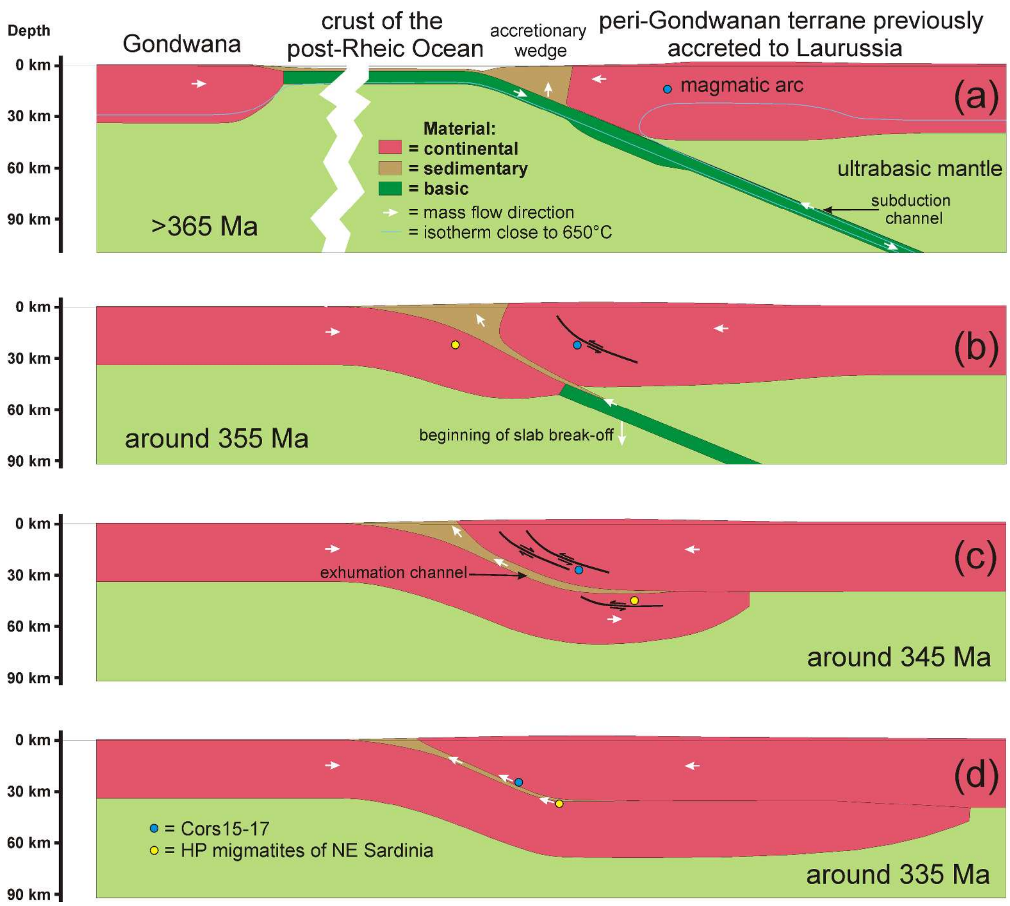
Depth
Gondwana
crust of the post-Rheic Ocean
accretionary wedge
peri-Gondwanan terrane previously accreted to Laurussia
0 km
30 km
60 km
90 km
magmatic arc
(a)
Material:
= continental
= sedimentary
= basic
= mass flow direction
= isotherm close to 650°C
ultrabasic mantle
subduction channel
>365 Ma
(b)
around 355 Ma
beginning of slab break-off
(c)
exhumation channel
around 345 Ma
(d)
= Cors15-17
= HP migmatites of NE Sardinia
around 335 Ma

Figure 11

**Table 1.** Representative analyses (in wt%) of garnet in the studied micaschists using an EMP. Twenty-four oxygen anions (double formula unit), a cation sum of Al + Ca + Cr + Fe + Mg + Mn + Na = 10, and the relation $Fe^{3+}$ = 4- (Al+Cr) were considered to calculate the structural formula of garnet. i. = inner, o. = outer, $XFe^{2+}$, XCa, XMg, and XMn are molar fractions of the garnet components Alm = almandine, Gro = grossular, Pyr = pyrope, Spe = spessartine.

| **sample** | | **Cors15G** | | | | **Cors17** | | |
|---|---|---|---|---|---|---|---|---|
| analysis No. | 0312-11 | 0312-3 | 0312-1 | 1411-6 | 1711-46 | 1711-54 | 1711-62 | 1711-68 |
| comment | i. core | o. core | mantle | rim | core | i. mantle | o. mantle | rim |
| $SiO_2$ | 37.49 | 37.37 | 37.41 | 37.01 | 37.07 | 37.17 | 36.54 | 36.74 |
| $TiO_2$ | 0.05 | 0.01 | 0.01 | 0.05 | 0.02 | 0.00 | 0.02 | 0.00 |
| $Al_2O_3$ | 21.39 | 21.28 | 21.49 | 21.00 | 21.06 | 21.15 | 21.11 | 21.54 |
| $Cr_2O_3$ | 0.01 | 0.03 | 0.00 | 0.01 | 0.01 | 0.03 | 0.01 | 0.00 |
| $Fe_2O_3$ | 0.34 | 0.76 | 0.58 | 0.06 | 0.39 | 0.31 | 0.40 | 0.00 |
| FeO | 31.96 | 33.30 | 34.46 | 31.41 | 32.98 | 31.70 | 31.86 | 32.43 |
| MnO | 5.21 | 3.29 | 2.87 | 8.03 | 4.56 | 5.89 | 6.52 | 6.88 |
| MgO | 3.62 | 4.13 | 3.85 | 1.56 | 3.15 | 2.97 | 2.73 | 2.51 |
| CaO | 1.51 | 1.56 | 1.49 | 1.62 | 1.43 | 1.68 | 1.41 | 0.88 |
| $Na_2O$ | 0.03 | 0.03 | 0.03 | 0.04 | 0.00 | 0.03 | 0.02 | 0.01 |
| Total | 101.63 | 101.75 | 102.20 | 100.79 | 100.65 | 100.94 | 100.62 | 101.00 |
| Si | 5.885 | 5.821 | 5.808 | 5.969 | 5.904 | 5.904 | 5.804 | 5.826 |
| Ti | 0.006 | 0.001 | 0.002 | 0.005 | 0.002 | 0.000 | 0.002 | 0.000 |
| Al | 3.958 | 3.908 | 3.932 | 3.991 | 3.953 | 3.959 | 3.951 | 4.027 |
| Cr | 0.002 | 0.003 | 0.000 | 0.002 | 0.001 | 0.003 | 0.002 | 0.000 |
| $Fe^{3+}$ | 0.040 | 0.089 | 0.067 | 0.008 | 0.046 | 0.037 | 0.047 | 0.000 |
| $Fe^{2+}$ | 4.196 | 4.339 | 4.474 | 4.235 | 4.394 | 4.211 | 4.231 | 4.301 |
| Mg | 0.848 | 0.958 | 0.892 | 0.376 | 0.747 | 0.702 | 0.647 | 0.593 |
| Mn | 0.693 | 0.434 | 0.378 | 1.097 | 0.615 | 0.793 | 0.877 | 0.924 |
| Ca | 0.255 | 0.260 | 0.249 | 0.279 | 0.244 | 0.286 | 0.240 | 0.150 |
| Na | 0.008 | 0.009 | 0.008 | 0.013 | 0.000 | 0.008 | 0.005 | 0.005 |
| Alm = $XFe^{2+}$ | 0.6993 | 0.7231 | 0.7456 | 0.7059 | 0.7323 | 0.7018 | 0.7052 | 0.7200 |
| Gro = XCa | 0.0424 | 0.0433 | 0.0414 | 0.0465 | 0.0407 | 0.0477 | 0.0399 | 0.0251 |
| Pyr = XMg | 0.1413 | 0.1597 | 0.1486 | 0.0626 | 0.1245 | 0.1171 | 0.1078 | 0.0993 |
| Spe = XMn | 0.1155 | 0.0723 | 0.0630 | 0.1828 | 0.1025 | 0.1321 | 0.1462 | 0.1548 |

**Table 2.** Representative analyses (in wt%) of diverse minerals in the studied micaschists using an EMP. The total was corrected for F. The structural formulae of the minerals were calculated as follows: muscovite (double formula unit) = 22-(1+Ca+Ba) O and (to calculate $Fe^{3+}$) Si+Ti+Al+Fe+Mn+Mg ≤ 4.10 (see Massonne & Schreyer, 1986); biotite = 11 O; feldspar = 8 O; sillimanite = 3 cations. $H_2O$ was calculated.

| **sample** | | | **Cors15G** | | | | | | **Cors17** | | |
|---|---|---|---|---|---|---|---|---|---|---|---|
| mineral | muscovite | | biotite | plagioclase | sillimanite | muscovite | | biotite | | plagioclase | K-feldspar |
| analysis No. | 2611-64 | 2611-51 | 2611-59 | 2611-53 | 1411-18 | 2611-16 | 2611-3 | 2611-18 | 2611-21 | 2611-34 | 2611-8 |
| comment | large | very small | | | | Ti-rich | Ti-poor | Ti-rich | Ti-poor | | |
| $SiO_2$ | 45.58 | 47.55 | 34.41 | 62.81 | 37.35 | 45.50 | 46.49 | 34.65 | 35.11 | 64.55 | 63.49 |
| $TiO_2$ | 0.87 | 0.13 | 2.69 | 0.00 | 0.00 | 0.83 | 0.03 | 2.42 | 1.04 | 0.00 | 0.02 |
| $Al_2O_3$ | 35.51 | 33.19 | 20.30 | 23.68 | 63.20 | 35.62 | 34.38 | 19.58 | 20.88 | 22.78 | 18.18 |
| $Cr_2O_3$ | | | | | 0.04 | | | | | | |
| FeO | 1.04 | 2.35 | 21.30 | | | 1.00 | 1.99 | 21.38 | 20.95 | | |
| $Fe_2O_3$ | 0.00 | 0.00 | | 0.02 | 0.15 | 0.00 | 0.03 | | | 0.01 | 0.38 |
| MnO | 0.02 | 0.07 | 0.26 | 0.00 | 0.00 | 0.03 | 0.00 | 0.23 | 0.15 | 0.00 | 0.00 |
| MgO | 0.73 | 1.60 | 7.40 | | | 0.63 | 1.42 | 8.33 | 8.67 | | |
| CaO | 0.01 | 0.10 | 0.00 | 4.57 | | 0.00 | 0.01 | 0.01 | 0.00 | 3.41 | 0.00 |
| $Na_2O$ | 0.58 | 0.18 | 0.16 | 8.92 | | 0.87 | 0.41 | 0.09 | 0.14 | 9.62 | 0.11 |
| $K_2O$ | 10.97 | 10.45 | 9.84 | 0.39 | | 10.31 | 10.64 | 9.25 | 9.50 | 0.23 | 16.70 |
| BaO | 0.34 | 0.13 | 0.13 | 0.00 | | 0.26 | 0.14 | 0.06 | 0.05 | 0.00 | 1.05 |
| F | 0.08 | 0.07 | 0.05 | | | 0.13 | 0.00 | 0.13 | 0.19 | | |
| $H_2O$ | 4.45 | 4.49 | 3.91 | | | 4.42 | 4.50 | 3.87 | 3.88 | | |
| Total | 100.16 | 100.28 | 100.43 | 100.40 | 100.75 | 99.54 | 100.04 | 99.94 | 100.48 | 100.61 | 99.93 |
| | | | | | | | | | | | |
| Si | 6.088 | 6.305 | 2.623 | 2.771 | 1.001 | 6.085 | 6.193 | 2.646 | 2.655 | 2.829 | 2.975 |
| Al | 5.590 | 5.186 | 1.824 | 1.231 | 1.995 | 5.615 | 5.397 | 1.762 | 1.404 | 1.177 | 1.004 |
| Ti | 0.087 | 0.013 | 0.154 | 0.000 | 0.000 | 0.084 | 0.003 | 0.139 | 0.515 | 0.000 | 0.001 |
| Cr | | | | | 0.001 | | | | | | |
| $Fe^{2+}$ | 0.116 | 0.260 | 1.358 | | | 0.112 | 0.222 | 1.365 | 1.325 | | |
| $Fe^{3+}$ | 0.000 | 0.000 | | 0.001 | 0.003 | 0.000 | 0.003 | | | 0.000 | 0.013 |
| Mn | 0.003 | 0.008 | 0.017 | 0.000 | 0.000 | 0.004 | 0.000 | 0.015 | 0.010 | 0.000 | 0.000 |
| Mg | 0.146 | 0.317 | 0.841 | | | 0.125 | 0.283 | 0.948 | 0.977 | | |
| Ca | 0.001 | 0.014 | 0.000 | 0.216 | | 0.000 | 0.002 | 0.001 | 0.000 | 0.160 | 0.000 |
| Ba | 0.018 | 0.007 | 0.004 | 0.000 | | 0.013 | 0.007 | 0.002 | 0.021 | 0.000 | 0.019 |
| Na | 0.149 | 0.047 | 0.023 | 0.763 | | 0.226 | 0.105 | 0.014 | 0.917 | 0.817 | 0.010 |
| K | 1.870 | 1.768 | 0.957 | 0.022 | | 1.758 | 1.807 | 0.901 | 0.001 | 0.013 | 0.998 |
| F | 0.032 | 0.031 | 0.012 | | | 0.055 | 0.000 | 0.031 | 0.045 | | |
| H | 3.968 | 3.969 | 1.988 | | | 3.945 | 4.000 | 1.969 | 1.955 | | |

**Table 3.** Bulk-rock composition (in wt%) of micaschists from south-eastern Corsica determined with wavelength-dispersive X-ray fluorescence (XRF) spectrometry. Slightly modified compositions used for thermodynamic calculations with PERPLE_X are given. 0 or 5% of Fe is trivalent. Reduction of the CaO content, corresponding to two third of the phosphorus content being related to form apatite (Ap), is marked by 2/3 Ap. The "semi-dry" composition results in water undersaturated conditions during retrogression.

| **Sample** | **Cors15G** | | | | **Cors16** | **Cors17** | | | |
|---|---|---|---|---|---|---|---|---|---|
| | XRF | modified for PERPLE_X calculations | | | XRF | XRF | modified for PERPLE_X calculations | | |
| Comment | | 0%$Fe^{3+}$,2/3 Ap | 5%$Fe^{3+}$,2/3 Ap | semi-dry | | | 0%$Fe^{3+}$,no Ap | 5%$Fe^{3+}$,2/3 Ap | 5%$Fe^{3+}$,no Ap |
| $SiO_2$ | 66.131 | 64.400 | 64.382 | 66.467 | 60.386 | 69.882 | 67.731 | 67.803 | 67.714 |
| $TiO_2$ | 0.710 | 0.691 | 0.691 | 0.714 | 0.882 | 0.645 | 0.625 | 0.626 | 0.625 |
| $Al_2O_3$ | 17.328 | 16.874 | 16.870 | 17.416 | 22.576 | 15.631 | 15.150 | 15.166 | 15.146 |
| FeO | | 4.623 | 4.622 | 4.772 | | | 4.359 | 4.364 | 4.358 |
| $Fe_2O_3$ or $O_2$ | 5.276 | | 0.026 | | 6.195 | 4.998 | | 0.024 | 0.024 |
| MnO | 0.062 | 0.060 | 0.060 | 0.062 | 0.124 | 0.098 | 0.095 | 0.095 | 0.095 |
| MgO | 1.759 | 1.713 | 1.712 | 1.768 | 1.446 | 1.601 | 1.552 | 1.553 | 1.551 |
| CaO | 0.802 | 0.653 | 0.653 | 0.674 | 0.187 | 0.468 | 0.454 | 0.330 | 0.453 |
| $Na_2O$ | 1.753 | 1.707 | 1.707 | 1.762 | 0.953 | 1.898 | 1.840 | 1.842 | 1.839 |
| $K_2O$ | 4.393 | 4.278 | 4.277 | 4.415 | 4.407 | 3.296 | 3.195 | 3.198 | 3.194 |
| $H_2O$ | | 5.000 | 5.000 | 1.950 | | | 5.000 | 5.000 | 5.000 |
| $P_2O_5$ | 0.150 | | | | 0.063 | 0.097 | | | |
| SUM | 98.364 | 100.000 | 100.000 | 100.000 | 97.219 | 98.614 | 100.000 | 100.000 | 100.000 |

**Table 4.** Representative EMP analyses (in wt%) of monazite in micaschist samples Cors15G and Cors17. The structural formula of monazite is related to 4 O.

| **Sample** | **Cors15G** | | **Cors17** | |
|---|---|---|---|---|
| Grain | 12 | 16 | 2 | 11 |
| Analysis No. | 58 | 65 | 3 | 22 |
| | | | | |
| $SiO_2$ | 0.17 | 0.55 | 0.12 | 0.26 |
| $P_2O_5$ | 28.69 | 27.74 | 28.59 | 28.28 |
| $SO_3$ | 0.02 | 0.02 | 0.02 | 0.02 |
| CaO | 1.07 | 1.02 | 1.05 | 0.95 |
| $Y_2O_3$ | 2.68 | 0.02 | 2.59 | 0.15 |
| $La_2O_3$ | 13.34 | 15.52 | 13.22 | 14.20 |
| $Ce_2O_3$ | 27.53 | 29.35 | 27.87 | 30.14 |
| $Pr_2O_3$ | 2.94 | 3.02 | 2.92 | 3.14 |
| $Nd_2O_3$ | 11.07 | 10.98 | 10.98 | 12.04 |
| $Sm_2O_3$ | 1.81 | 1.56 | 1.84 | 2.18 |
| $Gd_2O_3$ | 1.59 | 0.60 | 1.54 | 1.04 |
| $Dy_2O_3$ | 0.84 | 0.10 | 0.80 | 0.20 |
| $Er_2O_3$ | 0.23 | 0.04 | 0.24 | 0.04 |
| PbO | 0.1046 | 0.1367 | 0.1187 | 0.0980 |
| $ThO_2$ | 5.16 | 6.44 | 4.70 | 4.47 |
| $UO_2$ | 0.48 | 0.94 | 0.93 | 0.74 |
| Sum | 97.73 | 98.02 | 97.52 | 97.95 |
| | | | | |
| Si | 0.0068 | 0.0226 | 0.0049 | 0.0104 |
| P | 0.9788 | 0.9612 | 0.9791 | 0.9746 |
| S | 0.0006 | 0.0005 | 0.0006 | 0.0005 |
| Ca | 0.0463 | 0.0445 | 0.0454 | 0.0415 |
| Y | 0.0575 | 0.0003 | 0.0557 | 0.0033 |
| La | 0.1982 | 0.2342 | 0.1973 | 0.2131 |
| Ce | 0.4061 | 0.4396 | 0.4127 | 0.4491 |
| Pr | 0.0432 | 0.0450 | 0.0430 | 0.0465 |
| Nd | 0.1593 | 0.1605 | 0.1586 | 0.1750 |
| Sm | 0.0252 | 0.0219 | 0.0257 | 0.0306 |
| Gd | 0.0213 | 0.0082 | 0.0207 | 0.0141 |
| Dy | 0.0110 | 0.0013 | 0.0104 | 0.0026 |
| Er | 0.0029 | 0.0005 | 0.0030 | 0.0005 |
| Pb | 0.0011 | 0.0015 | 0.0013 | 0.0011 |
| Th | 0.0474 | 0.0600 | 0.0432 | 0.0414 |
| U | 0.0043 | 0.0086 | 0.0084 | 0.0067 |
| | | | | |
| Age (Ma) | 368.6 | 340.3 | 363.5 | 337.0 |
| 1σ error | 7.2 | 5.2 | 6.3 | 6.9 |